Geophysical Journal International

Eikonal Tomography: Surface wave tomography by phase-front tracking across a regional broad-band seismic array

Journal:	*Geophysical Journal International*
Manuscript ID:	GJI-08-0341
Manuscript Type:	Research Paper
Date Submitted by the Author:	03-Jul-2008
Complete List of Authors:	Lin, Fan-Chi; University of Colorado at Boulder, Physics Ritzwoller, Michael; University of Colorado at Boulder, Department of Physics Snieder, Roel K.; Colorado School of Mines, Department of Geophysics
Keywords:	Seismic tomography < SEISMOLOGY, Surface waves and free oscillations < SEISMOLOGY, Seismic anisotropy < SEISMOLOGY, Wave propagation < SEISMOLOGY, Interferometry < GEOPHYSICAL METHODS, North America < GEOGRAPHIC LOCATION

Eikonal Tomography: Surface wave tomography by phase-front tracking across a regional broad-band seismic array

Fan-Chi Lin[1], Michael H. Ritzwoller[1], and Roel Snieder[2]

1 - Center for Imaging the Earth's Interior, Department of Physics, University of Colorado at Boulder 80309-0390 (fanchi.lin@colorado.edu)

2 – Center for Wave Phenomena and Department of Geophysics, Colorado School of Mines, Golden, CO 80401

Abstract

We present a new method of surface wave tomography based on applying the Eikonal equation to observed phase travel time surfaces computed from seismic ambient noise. The source-receiver reciprocity in the ambient noise method implies that each station can be considered to be an effective source and the phase travel time between that source and all other stations is used to track the phase front and construct the phase travel time surface. Assuming that the amplitude of the waveform varies smoothly, the Eikonal equation states that the gradient of the phase travel time surface can be used to estimate both the local phase speed and the direction of wave propagation. For each location, we statistically summarize the distribution of azimuthally dependent phase speed measurements based on the phase travel time surfaces centered on different effective source locations to estimate both the isotropic and azimuthally anisotropic phase speeds and their uncertainties. Examples are presented for the 12 and 24 sec Rayleigh waves for the EarthScope/USArray Transportable Array stations in the western US. We show that: (i) the major resulting tomographic features are consistent with traditional inversion methods; (ii) reliable uncertainties can be estimated for both the isotropic and anisotropic phase speeds; (iii) resolution can be approximated by the coherence length of the phase speed measurements and is about equal to the station spacing; (iv) no explicit regularization is required in the inversion process; and (v) azimuthally dependent phase speed anisotropy can be observed directly without ad-hoc assumptions concerning its parametric form.

1. Introduction

The seismic surface wave tomography inverse problem is normally approached in one of two ways that can be thought of as either "single-station" or "array-based" methods. Both methods have proven effective at revealing the spatial variability of surface wave speeds from global to regional scales.

The first (single-station) approach to surface wave tomography is based on travel time measurements between a set of seismic sources (typically earthquakes) and a set of receivers one receiver at a time. The travel times are then interpreted in terms of wave speeds in the medium of propagation using ray theory with straight or potentially bent rays (e.g., Trampert and Woodhouse, 1996; Ekstrom et al., 1997; Ritzwoller and Levshin, 1998; Yoshizawa and Kennett, 2002) or finite frequency kernels (e.g. Dahlen et al., 2000; Ritzwoller *et al.* 2002; Levshin et al., 2005). This method results in a set of frequency-dependent dispersion maps of either Rayleigh or Love wave group or phase speed. This approach also has been applied to ambient noise data (e.g. Sabra et al., 2005; Shapiro et al., 2005; Yao *et al.* 2006; Moschetti et al., 2007; Lin *et al.* 2007; Yang et al., 2007; Bensen et al., 2008), which provides wave travel times between pairs of receivers. In this case, one station can be considered to be an "effective" source, but it is equivalent to the earthquake tomography problem with the effective sources exciting the wavefield. A variant of this method involves waveform fitting which in some cases bypasses the dispersion maps to construct the 3-D variation of shear wave speed directly in earth's interior (e.g. Woodhouse & Dziewonski 1984; Nolet, 1990; van der Lee and Fredriksen, 2005).

The second approach to surface wave tomography deals with stations as components of an array and interprets the phase difference observed between waves recorded across the array in terms of the dispersion characteristics of the medium. In doing so the method either applies geometrical constraints on the stations, typically that they lie nearly along a great circle with the earthquake (e.g. Brisbourne & Stuart 1998; Prindle & Tanimoto 2006), or inverts for the characteristics of the incoming wave-front along with the surface

wave dispersion characteristics of the medium lying within the array (e.g. Alsina *et al.* 1993; Friederich 1998; Yang & Forsyth 2006).

In both approaches, the surface wave dispersion maps result from a regularized inverse problem that is typically solved by matrix inversion. Regularization in most cases is ad-hoc, and includes spatial smoothing as well as matrix damping. As in many geophysical inverse problems, a trade-off between the amplitude of the heterogeneity and the resolution emerges that affects confidence in the smaller structural scales. This trade-off is most severe for azimuthal anisotropy in which the amplitude of anisotropy is particularly poorly determined (Laske & Master 1998; Smith et al., 2004; Deschamps *et al.* 2008). These problems are exacerbated by the fact that uncertainty information that emerges for the maps tends to be unreliable. Theoretical approximations made in the inversion, such as the assumption of straight (great-circle) rays or approximate sensitivity kernels, also affect the quality of the resulting maps. This particularly calls into question the robustness of information about azimuthal anisotropy because the magnitude of the travel time effects of azimuthal anisotropy and ray bending, for example, is similar.

The purpose of this paper is to present a new method of surface wave tomography that complements the traditional methods. The method is based on tracking surface wavefronts across an array of seismometers (Pollitz 2008) and should, therefore, be seen to lie within the tradition of array-based methods, although as will be seen in the discussion below the method degenerates to phase measurements obtained at single stations. The method is applicable, in principle, to surface waves generated both by earthquakes and ambient noise, but applications in this paper will concentrate on ambient noise recordings across the Transportable Array (TA) component of EarthScope/USArray (Fig. 1). Because it is an array-based method, however, an array is needed. The TA provides an ideal setting, but large PASSCAL experiments are suitable for the method and the emergence of large-scale arrays in Europe and China that mimic the TA also provide nearly optimal targets.

The method described in this paper is performed in three steps. We discuss the method

here in the context of ambient noise tomography such that each station can be considered to be an effective source as well as a receiver. The relevance of the method to earthquake tomography is discussed later in the paper. In the first step, a phase delay (or travel time) surface is computed across the array centered on each station. We refer to this step as wavefront or phase-front tracking. In the second step, the gradient of each travel time surface is computed at each spatial node. Invoking the Eikonal equation, the magnitude of the gradient is equal to local phase slowness and the direction of the gradient is the direction of propagation of the geometrical ray. Steps 1 and 2 are performed with every station in the array as the effective source at the center of the travel time surface. Finally, in step 3, for each spatial node the local phase speeds and wave path directions are compiled and averaged from the results centered on each individual station in the array. Because step 2 invokes the Eikonal equation, we refer to the method as "Eikonal tomography".

Eikonal tomography complements traditional surface wave tomography in several ways. First, there is no explicit regularization and, hence, the method is largely free from ad-hoc choices . The method as we implement it does, however involve smoothing in tracking the phase-fronts. Second, the method accounts for bent rays, but ray tracing is not needed. The gradient of the phase front provides information about the local direction of travel of the wave. The use of bent rays in traditional tomography necessitates iteration with ray tracing performed on each iteration. Third, the method naturally generates error estimates on the resulting phase speed maps. In our opinion, this is more useful than reliance on global misfit obtained by traditional inversion methods. Fourth, in the context of estimating azimuthal anisotropy, Eikonal tomography directly measures azimuth dependent phase velocities at each node. Unlike the traditional tomographic method, no ad-hoc assumption about the azimuthal dependency of the phase velocity is made. Finally, in the construction of phase speed maps, the ray tracing and matrix construction and inversion of the traditional methods have been replaced by surface fitting, computation of gradients, and averaging. The method, therefore, is computationally very fast and parallelizes trivially.

Although we have applied Eikonal tomography successfully from 8 sec to 40 sec period across the western US, we present results here only for the 12 sec and 24 sec Rayleigh waves. In principle, the same method can be applied to Love waves as well. The results shown in this study are presented to illustrate the method. Interpretation of the results will be the subject of future contributions.

2. Theoretical Preliminaries

The traditional approach to seismic tomography begins with a statement of the forward problem that links unknown earth functionals (such as seismic wave speeds, surface wave phase or group speeds, etc.) with observations. In surface wave tomography, when mode coupling and the directionality of scattering are neglected, this involves the computation of travel times from the 2-D distribution of (frequency dependent) surface wave phase speeds, $c(\mathbf{r})$, that can be written in integral form as

$$t(\mathbf{r}_s, \mathbf{r}_r) = \int A(\mathbf{r}, r_s, \mathbf{r}_r) \frac{dx^m}{c(\mathbf{r})} \qquad (1)$$

where $\mathbf{r_S}$ and $\mathbf{r_r}$ are the source and receiver locations, $\mathbf{r}$ is an arbitrary point in the medium, and *m = 1 or 2* denotes line and area integrals, respectively. For "ray theories", *m = 1* and the integral kernel, $A(\mathbf{r},\mathbf{r}_s,\mathbf{r}_r)$, vanishes except along the path, which is typically either a great-circle (straight ray) or a path determined by the spatial distribution of phase speed (geometrical ray theory) that is known only approximately. Ray theories are fully accurate at infinite frequency and approximate at any finite frequency. For *m = 2*, the integral is over area, and the integral kernel represents the frequency dependent finite spatial extent of structural sensitivity. The sensitivity kernel may be ad-hoc (e.g., Gaussian beam) or determined from a scattering theory (e.g, Born/Rytov) given a particular 1D or higher dimensional input model. Spatially extended kernels are referred to as finite frequency kernels, to contrast them with ray theories. Much of the theoretical work in surface wave seismology has been devoted to developing increasingly sophisticated, and presumably accurate, representations of the integral kernel in equation (1) (e.g.

Zhou *et al.* 2004; Tromp *et al*. 2005), although debate continues about whether approximate finite frequency kernels are preferable to ray theories based on bent rays with ad-hoc cross-sections (e.g., Yoshizawa and Kennett, 2002; van der Hilst & de Hoop 2005; Montelli *et al*. 2006; Trampert and Spetzler, 2006).

Equation (1) defines travel time as a "global" constraint on structure; that is, it is a variable that depends on the unknown structure over an extended region of model space and is defined to be contrasted with "local" constraints. The traditional primacy of the forward problem in defining the inverse problem necessitates that the inverse problem is similarly global in character. Travel time observations constrain phase speeds non-locally, that is over an extended region of model space.

In contrast, Eikonal tomography places the inverse problem in the primary role once the phase travel time surfaces, $\tau(\boldsymbol{r_i}, \boldsymbol{r})$, for positions $\mathbf{r}$ relative to effective sources located at $\boldsymbol{r_i}$ are known. The Eikonal equation (e.g., Wielandt 1993; Shearer, 1999) is based on the following

$$\nabla \tau(\boldsymbol{r}_i, \boldsymbol{r}) = \frac{\hat{\mathbf{k}}_i}{c_i(\boldsymbol{r})} + O\left[\left(\frac{\nabla^2 A}{A\omega^2}\right)^{1/2}\right] \qquad (2)$$

which is derived directly from the Helmholtz equation. Here, c_i is the phase speed for travel time surface i at position $\mathbf{r}$ and $\hat{\mathbf{k}}_i$ is the unit wave number vector for that travel time surface at position $\boldsymbol{r}$. The gradient is computed relative to the field vector $\boldsymbol{r}$, ω is frequency, and A is the amplitude of an elastic wave at position $\boldsymbol{r}$. The Eikonal equation derives by ignoring the second term on the right hand side. In this case, the magnitude of the gradient of the phase travel time is simply related to the *local* phase slowness at $\mathbf{r}$ and the direction of the gradient provides the *local* direction of propagation of the wave. Thus, the Eikonal equation places local constraints on the surface wave speed.

Dropping the second term on the right hand side of equation (2) is justified either at high

frequencies or if the spatial variation of the amplitude field is small. The latter is the less restrictive constraint and will hold if lateral phase speed variations are sufficiently smooth to produce a relatively smooth amplitude field. Moreover, when repeated measurements are performed with different phase travel time surfaces, the errors due to dropping the amplitude term will be unlikely to constructively interfere to produce a systematic bias but will contribute to the estimated uncertainty especially when the wavelength is shorter than the dimension of velocity structure (Bodin & Maupin 2008). We take this interpretation as the basis for the use of the Eikonal equation. In addition, in ambient noise tomography absolute amplitude information is typically lost due to time- and frequency-domain normalization prior to cross-correlation. In this circumstance, the computation of the second term on the right hand side of equation (2) is impossible.

The question may arise whether Eikonal tomography should be considered to be a geometrical ray theory or a finite frequency theory. The question is motivated by considering globally constrained inverse problems and is somewhat ill-posed for the locally constrained inversion. We believe, however, that the answer is that Eikonal tomography has elements of both. Certainly, the Eikonal equation presents information about the local direction of propagation of a wave and is, therefore, not a straight ray method but is "geometrical" in character. But, the phase travel time surfaces that are taken as data in the inversion possess spatially extended sensitivity (finite frequency information) and Lin and Ritzwoller (*On the determination of empirical surface wave sensitivity kernels*, manuscript in preparation, 2008) shows how approximate empirical finite frequency kernels can be determined from them. Thus, ignoring the second term on the right hand side of equation (2) does not equate with rejecting finite frequency information. However, the resulting interpretation of the local gradient of the phase travel time surface in terms of a wave with a single well-defined direction, $\hat{\mathbf{k}}$, is consistent with a single forward scatterer approximation. If there were more than one scatterer, i.e., multipathing, then the equation could not be interpreted as defining an unambiguous direction of travel at each point. Thus, we do not see Eikonal tomography as a ray method, but summarize it as an approximate finite frequency, geometrical (i.e., bent ray), single forward scatterer method.

3. Phase-front Tracking

Eikonal tomography for ambient noise begins by constructing cross-correlations between each station-pair. The ambient noise cross-correlation method to estimate the Rayleigh wave empirical Green's functions (EGFs) is described by Bensen et al. (2007) and Lin et al. (2008). We use the method to produce EGFs and phase velocity curves between 8 and 40 sec period and have processed all available vertical component records from the USArray/TA observed between October 2004 and November 2007. These stations are shown in Figure 1. The symmetric component cross-correlation between each station pair is used to construct the EGFs.

Each phase travel time surface is defined relative to a given station location, $\mathbf{r}_i$. If $\mathbf{r}$ denotes an arbitrary location, then the travel time surface relative to effective source i is given by $\tau(\mathbf{r_i}, \mathbf{r})$ for $1 \leq i \leq n$, where n is the number of stations. The construction of the phase travel time surfaces across the array starts by mapping the phase travel times in space centered on each station. Figure 2a presents example great-circle ray paths for an effective source at TA station R06C and Figure 2b shows the EGFs to all other TA stations plotted as a record section band-pass filtered from 15 to 30 sec period. The coherence of the information contained in this record section can be seen in wavefield snap-shots such as those in Figure 3, in which the amplitude of the envelope function for each EGF is color coded. Plots such as these and many others illustrate that the entire Rayleigh wavefield can be seen to propagate away from the effective source. The plot also illustrates how the amplitude of the EGF varies with azimuth, with the largest amplitude pointing directly toward or away from the coast relative to the central station. Nevertheless, reliable phase times are measurable at all azimuths, which is essential in order to map the phase travel time surface.

Phase travel times to all stations from an effective source are measured using the method of Lin et al. (2008) on each EGF between 8 and 40 sec period. For a fixed frequency, the measured phase travel time is assigned to each station whose EGF has a signal-to-noise

ratio (SNR) exceeding 15, where SNR is defined by Bensen et al. (2007). To construct a phase travel time surface, these phase travel times must be interpolated onto a finer, regular grid. To do this, we fit a minimum curvature surface onto a 0.2°x0.2° grid across the western US. The result for central station R06A for the 24 sec Rayleigh wave is shown in Figure 4a. Variations in the method of interpolation have minimal effect on the resulting surface averaging less than 0.2 sec except near the central station and on the map's periphery. An example is shown in Figure 4b in which the second interpolation scheme invokes an extra tension term in the surface fitting (Smith and Wesson, 1990). The difference near the center is expected because the real travel time surface will have singular curvature at the effective source. Accurate modeling of the phase time surface near the source, therefore, would require a different method of interpolation than that used here. In addition, travel time measurements obtained between stations separated by less than 1-2 wavelengths are less reliable than those from longer paths. Thus, from each travel time surface we remove the region within two wavelengths of the central station and also any region in which the phase travel time difference between the two interpolation methods is greater than 1.0 sec. Finally, as an added quality control measure, for each location we include measurements from this location only when at least three of the four quadrants of the East-West and North-South axes are occupied by at least one station within 150 km. The resulting truncated phase travel time map centered on station R06A for the 24 sec Rayleigh wave is shown in Figure 5a. Several other examples with either a difference central station or a different period are also shown in Figure 5. The method of phase front tracking is not perfect, as several irregularities in the contours of constant travel time in Figure 5c testify. Statistical averaging is needed to reduce the effects of these irregularities, as discussed later in section 4.

The phase-front tracking process introduced here is essentially the only place in the Eikonal tomography where the inverter has the freedom to make ad-hoc choices. The choice of using minimum curvature surface fitting method as our interpolation scheme minimizes the variation of the gradient and hence gives the smoothest resulting velocity variation. With this interpolation scheme, however, the phase travel time surface within an area confined within three to four closest stations will always have similar gradients.

This spatial coherence of the variation of the gradient, as we will discuss later on, limits our ability to resolve velocity anomalies much smaller than the station spacing. If higher resolution is desired, a more sophisticated interpolation scheme will be required.

4. Eikonal Tomography

From equation (2), the Eikonal equation is written

$$\nabla \tau(\mathbf{r}_i, \mathbf{r}) = \frac{\hat{\mathbf{k}}_i}{c_i(\mathbf{r})} \qquad (3)$$

The magnitude of the gradient of the phase travel time, therefore, is simply related to the local phase slowness at **r** and the direction of the gradient provides the direction of propagation of the wave. Taking the gradient on the phase travel time surface gives the local phase speed as a function of the direction of propagation of the wave, hence there is no need for a tomographic inversion. If the Eikonal equation is looked at as an inverse problem, the gradient is seen as the inverse operator that maps travel time observations into model values (phase slownesses) and is applied without the need first to construct the forward operator.

4.1 Isotropic wave speeds

Figure 6 shows the result of applying the Eikonal equation to the phase travel time surface for the 24 sec Rayleigh wave shown in Figure 5a centered on station R06A. For each individual central station *i*, the resulting phase speed map is noisy (Figure 6a) due to imperfections in the phase travel time map. This is caused by errors in the input phase travel times which, in a similar measurement, Lin et al. (2008) estimated to be about 1 sec, on average. This is a significant error when spacing between stations is small. But, there are *n* stations, which in the present study for the TA is about 490. This allows the statistics of the phase speed estimates to be determined. For example, Figure 7a shows the 455 Rayleigh wave phase speed measurements at a period of 24 sec as a function of

propagation direction for the point in Nevada identified by the star in Figure 1. To determine the isotropic phase speed and its uncertainty for each point, we first calculate the mean slowness, s_0, and the standard deviation of the mean slowness, σ_s, from the distribution of measurements:

$$s_0 = \frac{1}{n}\sum_{i=1}^{n} s_i \tag{4}$$

$$\sigma_s^{\,2} = \frac{1}{n(n-1)}\sum_{i=1}^{n}(s_i - s_0)^2 \tag{5}$$

This intermediate step properly accounts for error propagation. The isotropic phase speed, c_0, and its uncertainty, σ_c, are then determined by

$$c_0 = \frac{1}{s_0} \tag{6}$$

$$\sigma_c = \frac{1}{s_0^{\,2}}\sigma_s \tag{7}$$

The local uncertainty σ_c is mapped for the 24 sec Rayleigh wave in Figure 8a where only the region in which the number of measurements is greater than half the total number of the effective sources is shown. The average uncertainty across the map is about 7 m/sec or about 0.2% of the phase speed.

Example phase speed measurements and the uncertainty map for the 12 sec period Rayleigh wave are displayed in Figure 7b and 8b respectively. Uncertainty at this period is largest along the western and northern edges of the region which is most likely due to small scale wave-front distortion resulting from large velocity contrasts. The average uncertainty is about 8 m/sec, which is slightly larger than at 24 sec. This is not unexpected, because the validity of the Eikonal equation relies on smoothly varying velocity structures and this is a less robust assumption for surface waves at shorter periods.

The isotropic phase speed maps at periods of 24 sec and 12 sec are plotted in Figures 9a and 10a, respectively. For comparison, the phase speed maps determined from the phase

speed measurements using our traditional tomographic method based on a straight ray inversion method (Barmin et al., 2001) are shown in Figures 9b and 10b. Differences between the methods are illustrated in Figures 9c and 10c.

Agreement between the isotropic maps produced with Eikonal tomography and traditional straight ray tomography is generally favorable, but there are regions of significant disagreement. At 24 sec period, the differences are greatest near the western boundary of the map where Eikonal tomography seems to recover crisper, more highly resolved features that correlate better with known geological structures. For the 24 sec Rayleigh wave, the phase velocity contrast between the fast and slow anomalies is generally too gentle to make ray paths deviate significantly from great circle paths. This is also indicated in Figure 6b where the average deviation of propagation direction from great circle path is about 3°. It is not likely, therefore, that the differences observed between Eikonal and traditional tomography at this period are purely because Eikonal tomography accounts for bent rays. Differences more likely result from the regularization applied in the straight ray inversion, which tends to distort the velocity anomalies near the edges of the map. At 12 sec period, however, velocity contrasts are more significant and the off-great-circle effect is more important. The effect of modeling bent rays in Eikonal tomography can be seen in at least two features of the 12 sec maps. First, a lineated anomaly associated with the Cascade Range is better observed with Eikonal tomography. Second, Eikonal tomography also produces wave speeds that are systematically slower than the straight ray inversion (Figure 10c) in most of the region. The bent rays travel faster than the straight rays (Roth *et al.* 1993) and to fit the data equally well with bent rays requires depression of wave speeds, on average. This can be seen clearly in the histograms of differences presented in Figure 11, where the mean difference between the two 12 sec maps is about 10 m/sec (~0.3%), whereas the 24 sec maps differ, on average, only by ~5 m/sec.

4.2 Resolution: coherence length of the measurements

Traditional estimates of resolution typically are based on applying the inverse operator

(relating observations to model variables) to the forward operator (relating model variables to observations) in an inverse problem. With Eikonal tomography, neither an inverse nor a forward operator are constructed explicitly, so resolution is not straightforward to determine. Checkerboard tests are possible, but numerical simulations would need to accurately calculate the phase travel time between each station pair.

We take a different approach and attempt to estimate the resolution based on the coherence length of the measurements. To do so, we first estimate the statistical correlation, ρ, of slowness measurements between locations, j and k, by

$$\rho_{jk} = \frac{\left(\sum_{i=1}^{n}(s_{ji} - s_{j0})(s_{ki} - s_{k0})\right)^2}{\sum_{i=1}^{n}(s_{ji} - s_{j0})^2 \sum_{i=1}^{n}(s_{ki} - s_{k0})^2} \quad (8)$$

where i is the index of the effective sources and s_{j0} and s_{k0} are the mean slowness at locations j and k, respectively. The statistical correlation, ρ, varies between 0 and 1 and represents the degree of coherence between the measurements made at the two locations. Using the point in central Nevada (Figure 1) as an example again, the statistical correlation between the phase speed observations at that point and the neighboring points is summarized as a correlation surface shown in Figure 12a. We follow Barmin *et al.* (2001) and estimate the "resolution" by fitting the correlation surface with a cone (Figure 12b), where the base radius of the cone is taken as the resolution estimate R.

Although this is different from the traditional definition of resolution, it does provide information on the length scale of features that can be resolved in a region. Resolution estimated in this way for the 24 sec Rayleigh wave is shown in Figure 12c. In most regions, resolution is slightly smaller than the average inter-station spacing of 70 km across the western US. Although this result is comparable to the result of straight ray tomography (Lin *et al.* 2008), there are fundamental differences between the two. When the observed phase travel times are affected by a velocity structure much smaller than the inter-station distance, without a more sophisticated interpolation scheme, the minimum

curvature fitting method we use will smear the travel time anomalies to an area confined by the few closest nearby stations. Thus, the station spacing constrains the possible resolution. We note that increasing the number of effective sources will probably reduce the estimated uncertainty, but most likely will have little impact on the resolution. In traditional methods, the resolution is mainly controlled by the path or kernel density and the regularization that is imposed by the inverter. With dense path coverage, which is the case for our phase travel time dataset, unrealistically high resolution would be achieved with weak smoothing regularization in traditional tomography, but a patchy tomography result would be inevitable

4.3 Azimuthal anisotropy

Eikonal tomography also provides a method to estimate azimuthal anisotropy. In traditional surface wave inversions, it is commonly assumed that the Rayleigh wave phase speed exhibits the following azimuthal anisotropy in a weakly anisotropic medium (Smith & Dahlen 1973),

$$c(\psi) = c_0 + A \cos [2(\psi - \varphi)] + B \cos[4(\psi - \alpha)] \quad (9)$$

where ψ is the azimuthal angle measured positive clockwise from north, A and B are the amplitude of anisotropy, and φ and α define the orientation of the anisotropic fast axes for the 2ψ and 4ψ components of anisotropy. This parameterization, however, is valid for weak anisotropy only and may not hold for the actual dependence of velocity on azimuth. Moreover, although the estimated 2ψ fast directions may be robust in the traditional inversion, the amplitude of the anisotropy almost inevitably depends on the regularization parameters chosen. In our approach, we directly measure the velocity as a function of azimuth of the wave and then verify if the relationship reflects such a simple function of azimuth.

As with the isotropic phase velocity determination, the estimation of anisotropy begins with the set of phase speeds estimated at a single spatial location from the set of phase speed travel time maps segregated by azimuth, as in the example shown in Figure 7a for the 24 sec Rayleigh wave for a point in central Nevada. Due to phase travel time errors in the maps, the measured phase speeds are significant scattered and any azimuthally dependent trend is obscured. Scatter is reduced substantially by two stacking processes. First, we combine the azimuthally dependent phase speed measurements obtained at the target point with measurements at the eight surrounding spatial points (3x3 grid with the target point at the center). We use a 0.6^o grid separation approximately equal to the resolution estimate described in the last section, which effectively guarantees that measurements are statistically independent from one other. To reduce mapping the lateral variation of isotropic phase speed into azimuthal anisotropy, we remove the isotropic speed difference between each point and the center point of the 3x3 grid for all of the measurements. This stacking process increases the number of measurements for the center point, but at the expense of reducing spatial resolution. Second, we combine all of the azimuthally dependent phase speed measurements in each 20^o azimuthal bin into a mean speed and its uncertainty for that bin. Here, again, the mean slowness and the standard deviation of the mean slowness are first calculated and then converted to the mean speed and its uncertainty.

Figure 13 shows examples for four different geographical locations of the resulting stacked azimuthally dependent phase speed measurements with their uncertainties for the 24 sec Rayleigh wave. For the examples in Utah and Nevada, Figures 13a and b, where good azimuthal data coverage exists, a clear 2ψ variation is observed for the entire 360^o of azimuth. On the other hand, Figures 13c and d show two examples near the western boundary of the map where azimuthal coverage is limited. Although only part of the entire azimuth range has valid measurements, the 2ψ velocity signal is still observed robustly because measurements cover at least 180^o. Based on these observations, for each period and location, we fit the result with the 2ψ part of the cosinusoid and use it to estimate the amplitude and fast direction of anisotropy with associated uncertainties.

Adding the 4ψ term does not improve the data fit appreciably which indicates that the 4ψ variation of Rayleigh waves is probably weaker and our dataset is not sufficient to constrain it. The observed 2ψ azimuthal anisotropy exhibits different amplitudes and fast directions in different locations. This eliminates the concern about having systematic errors in the input phase travel times due to uneven ambient noise source distribution which should result in a uniform fast direction for the whole region.

Azimuthal anisotropy for the 24 sec Rayleigh wave in the whole region is summarized in Figure 14a. The peak-to-peak amplitude of anisotropy is presented in Figure 14b. Figure 15a presents the variance reduction after introducing the 2ψ anisotropy term. Significant improvements (>80%) are observed over extensive regions, which not only indicates the robustness of the measurements but also suggests that azimuthal anisotropy is a general feature which should not be overlooked. We note that the regions with poor variance reduction (<40%) are generally accompanied by weak anisotropy (<0.5%), which may be a real feature or may be due to a spatially rapid local change in fast directions. The estimated uncertainty of the observed azimuthal anisotropy fast directions and amplitudes are summarized in Figure 15b and c, respectively. As in the traditional anisotropy tomography, the fast directions are generally robust features. We estimate the uncertainties of the fast directions to be less than 6^{o} in most of regions. Again, regions with larger uncertainties in the fast direction generally result from weak anisotropy. Uncertainties in the amplitude of anisotropy are generally smaller (<4m/s or 0.1% of the isotropic phase speed) in regions with nearly complete azimuthal data coverage than near the periphery of the studied region where only part of entire azimuthal range has measurements.

For comparison, the 2ψ 24 sec Rayleigh wave phase speed anisotropy determined by traditional straight ray inversion (e.g., Barmin et al., 2001) with two different smoothing strengths are summarized in Figure 16a and 16d with amplitudes plotted in Figure 16b and 16e. The difference in fast directions compared to Eikonal tomography is also

summarized as histograms in Figure 16c and 16f, where only regions with anisotropy amplitude larger than 0.5% in the Eikonal tomography are included. Overall, the observed anisotropy fast direction patterns are consistent between the two traditional inversions and the Eikonal tomography inversion. This is not unexpected since the off-great-circle effect is relatively weak at this period. The anisotropy amplitude is significantly smaller in the second case of the straight ray inversion, which indicates that the smoothing regularization was too strong. Most places with a significant difference in fast directions (>30°) occur near a transition in the fast direction of anisotropy where the results of neither model are robust.

With the traditional inversion method, it is tricky to select the right regularization parameters and methods are typically ad-hoc. Many studies use trade-off curves between misfit and model roughness or the number of degrees of freedom to select the preferred regularization parameters (e.g. Boschi 2006; Zhou *et al.* 2005). This is, however, difficult for azimuthal anisotropy because by including 2ψ azimuthal anisotropy, for example, the number of degrees of freedom at each node increases to 3 from 1 for an isotropic speed inversion despite the fact that the improvement in misfit is usually modest. For traditional tomography applied to the 24 sec Rayleigh wave phase speed data, the standard deviation of travel time misfit drops from around 3 sec for a homogeneous reference model to 1.57 sec after the straight ray isotropic speed inversion (Figure 9b). However, it then only decreases slightly to 1.53 sec and 1.54 sec for the two 2ψ azimuthal anisotropy inversions (Figure 16a and 16d), producing a variance reduction less than 3%. With Eikonal tomography, we stack the azimuthally dependent phase speed measurements, interpret the observed anisotropy more intuitively, and achieve a variance reduction greater than 80% on average. Note that the variance reduction will be slim without the stacking processes, which is evidenced by the scattering of the phase speed measurements in Figure 7.

The 12 sec Rayleigh wave 2ψ azimuthal anisotropy results based on Eikonal tomography are presented in Figure 17. Overall, the anisotropy is robustly measured despite the fact

that the amplitudes of anisotropy are generally weaker and the fast direction pattern is slightly different from the 24 sec results. Figure 18a shows an example of 12 sec 2ψ azimuthal anisotropy determined by our traditional straight ray inversion with anisotropy amplitude plotted in Figure 18b. The difference in fast directions compared to the Eikonal tomography is summarized as the histograms in Figure 18c. Compared to 24 sec, more significant differences in both the fast directions and the amplitude patterns are observed, particularly near regions where there are discrepancies between the two isotropic speed maps (Figure 10). We believe that the off-great-circle effect, which should play a more important role for 12 sec Rayleigh waves, is responsible for most of the observed differences between the methods. Neglecting the fact that the wave does not follow the great-circle path can cause significant errors in the estimation of azimuth anisotropy.

5. Discussion

5.1 Advantages and limitations of Eikonal tomography

There are several significant advantages of Eikonal tomography over traditional surface wave tomography methods.

First, the implementation of inverse operator for Eikonal tomography depends on operations to the data without explicitly solving the forward problem. For a wave propagating in an inhomogeneous medium, the observed wave properties such as phase travel time are only linearly related to the local velocity structure when structural perturbations are small. In other words, any linearized forward operator, such as the ray integral or sensitivity integral, and the inverse operator derived from it can only be considered approximate. Errors caused by this linearization are often overlooked or are unknown, and moving beyond them requires iterative simulations which are computationally expensive. Eikonal tomography extracts the information about local velocity structure directly from the data without explicitly constructing the forward operator. It, therefore, finesses the nonlinear nature of the problem and should result in a better estimate of both the local isotropic and anisotropic phase speed, especially where

off-great-circle propagation is important.

Second, uncertainties in local phase speeds can be estimated with Eikonal tomography. Instead of minimizing a penalty functional that usually includes some combination of global misfit and model norm or roughness, Eikonal tomography directly estimates local phase speed from independent measurements based on different phase travel time surfaces. Therefore, the uncertainties of the resulting local phase speeds can be determined statistically in a straightforward way. The uncertainties are important for later 3D inversion and quantitative comparisons between different models.

Third, Eikonal tomography is free from explicit model regularization. The method, therefore, eliminates the need to make ad-hoc choices of the damping and regularization parameters which are sometimes controversial and may result in dubious models. This particularly is a problem for studies of surface wave azimuthal anisotropy because the increased number of degrees of freedom is often not offset by a comparable improvement in misfit. Eikonal tomography with the additional smoothly intrinsically embedded in the phase front tracking process has no explicit regularization and the subjectivity of the inverter to affect the tomographic result is restricted.

Fourth, the azimuthal dependence of phase speeds can be measured directly without ad-hoc assumptions concerning its parametric form. Unlike classic studies of Pn azimuthal anisotropy (e.g., Morris *et al*. 1969) where the wave speed variation with the direction of propagation is observed directly, traditional surface wave tomography typically posits the relationship between phase speed and the direction of wave propagation based on theoretical studies of weakly anisotropic media (e.g. Smith & Dahlen 1973). The ability to measure and see the azimuthal dependence of phase speeds directly leads to greater confidence in the information about anisotropy.

There are two limits on Eikonal tomography worthy of note. First, unlike traditional inversion methods where the resolution is controlled by path or kernel densities, the resolution limit in Eikonal tomography is controlled by station spacing. Without applying

a more sophisticated travel time surface interpolation method, this prohibits the use of this technique to resolve structures smaller than the given station spacing. Second, when long period or more complicated surface waves are considered, the second term in equation (2) can have values similar to the phase speed anomalies that we seek to resolve. Theoretical and numerical studies, such as Wielandt (1993) and Friederich *et al.* (2000), suggest that when either the velocity anomaly is smaller than a wavelength or the incoming wave is complicated by multipathing, neglecting the amplitude term by the Eikonal equation can blur the velocity anomaly and cause systematic errors in the phase speed measurements. It is possible to solve this problem by inverting both phase and amplitude together which amounts to recasting the problem in terms of the Helmholtz equation. Amplitude measurements are, however, less accurate than phase measurements and the second spatial derivative of the amplitude variation tends to be unstable. In this case, further smoothing would be required. The situation is even worse for measurements based on ambient noise cross-correlations where amplitudes have been separately normalized for different stations so that meaningful amplitude information has been lost. Amplitude anomalies mainly reflect the distribution of ambient noise sources not structural gradients.

The scattering observed in the distribution of local phase speed measurements, such as those shown in Figure 7, may partly be due to the neglect of the amplitude term in the Eikonal equation. We suspect, however, that its contribution is relatively small for the following reasons. First, considering the short distance between each effective source and each receiver, it is unlikely mutipathing will be well developed in the period band we consider (8 – 40 sec). Second, for this period range, the wavelength is genearlly smaller than the spatial scale of the inferred phase velocity structures (Figure 9a and 10a). Numerical simulations based on our isotropic phase speed maps also indicate that the errors due to neglecting the amplitude term in each of the local phase speed measurements is small (<0.5% of the input local speed). We believe, therefore, that the scattering observed in the distribution of local phase speed measurements principally reflects phase time measurement errors which are largely due to imperfections in the distribution of ambient noise sources.

5.2 Applicability to earthquake tomography

To construct the phase travel time surfaces in this study we use measurements of ambient noise. In principle, however, Eikonal tomography can be applied to phase travel time measurements based on earthquake waveforms. There are a few differences, however, considering the nature of earthquake measurements.

First, surface waves emitted by a distant source usually develop a certain amount of multipathing that can potentially invalidate the assumption of smoothly varying amplitudes. In fact, this is the fundamental concept of the two plane wave inversion method (e.g., Yang & Forsyth 2006). Friederich *et al.* (2000) showed numerically how wave complexity can contribute to uncertainties in the local phase speeds inferred from the Eikonal equation. This problem is relatively minor for measurements based on ambient noise cross-correlations because the effective sources (i.e., the stations in the ambient noise method) usually are located within the area of inversion and often the distance is too short for multipathing to be well developed. Second, surface wave studies based on teleseismic events usually focus on longer periods (>25 sec) due to the strong scattering and attenuation of shorter period signals. At longer periods, when a wavelength is larger than to the size of velocity anomaly structure, the second term in equation (2) can blur and distort the velocity anomaly that we wish to resolve (Friederich *et al.* 2000).

Considering these factors, the amplitude term may play a bigger role in the Eikonal tomography based on earthquake measurements and the second term in equation (2) must be properly taken into account. Unlike ambient noise cross-correlation measurements where only the phase information is available, the amplitude of the surface wave emitted by an earthquake can be used in the inversion as well. By including amplitude information, the Helmholtz equation can be applied instead of the Eikonal equation, and may resolve the local phase velocity structure with greater certainty (Wielandt 1993; Friederich *et al.* 2000).

6. Conclusions

We present a new method of surface wave tomography called Eikonal tomography and argue that this method presents an improvement over traditional methods of ambient noise tomography, particularly as the method is applied to data from the Transportable Array component of EarthScope/USArray. The method initiates by tracking phase fronts across the array to produce phase travel time maps centered on each station, considered as an "effective source". The method culminates by interpreting the local gradients of the phase time surfaces in terms of local phase speed and the direction of propagation of the wave.

The most significant advantages of Eikonal tomography compared with traditional straight-ray tomography is its more accurate representation of wave propagation, its ability to produce meaningful uncertainty information about the inferred phase speed maps, and its production of more reliable information about azimuthal anisotropy. Improvements in the isotropic dispersion maps result predominantly from the method's ability to track the direction of propagation of waves, which is tantamount to use of off-great-circle geometrical rays but without the need for iteration. Improvements in information about azimuthal anisotropy derive from the method's freedom from ad-hoc choices in regularization. This provides more reliable information about the amplitude of anisotropy, in particular. In addition, the method provides a local visualization of how phase speeds vary with azimuth, which we believe adds considerably to our confidence in the results.

Eikonal tomography is an approximate method. It accurately tracks the direction of wave propagation but only approximately incorporates what may be traditionally thought of as finite-frequency effects and assumes a single wave propagating at each point in space. Moving beyond application of the Eikonal equation will necessitate the computation of the second term in the right hand side of equation (2). At present, this is not feasible because absolute amplitude information is lost in ambient noise data processing. Future work naturally will attempt to retain amplitude information from ambient noise which will allow the magnitude and nature of this discarded term to be assessed quantitatively.

Acknowledgments

The data used in this research were obtained from the IRIS Data Management Center and originate predominantly from the Transportable Array component of EarthScope/USArray. Aspects of this research were supported by grants from the US National Science Foundation, grants EAR-0450082, EAR-0711526, and EAS-0609595, and a contract from the US Department of Energy, contract DE-FC52-2005NA2607.

References

Alsina, D., R. Snieder, and V. Maupin, 193, A test of the great circle approximation in the analysis of surface waves, *Geophys. Res. Lett.,* 20, 915-918.

Barmin, M.P., Ritzwoller, M.H. & Levshin, A.L., 2001. A fast and reliable method for surface wave tomography, *Pure Appl.Geophys.,* 158, 1351-1375.

Bensen, G.D., Ritzwoller, M.H., Barmin, M.P., Levshin, A.L., Lin, F., Moschetti, M.P., Shapiro, N.M., & Yang, Y., 2007. Processing seismic ambient noise data to obtain reliable broad-band surface wave dispersion measurements, *Geophys. J. Int.*, 169, 1239-1260.

Bensen, G.D., M.H. Ritzwoller, and N.M. Shapiro, 2008. Broad-band ambient noise surface wave tomography across the United Stated, *J. Geophys. Res.*, 113, B05306, 21 pages, doi:10.1029/2007JB005248.

Bodin, T. & Maupin, V., 2008. Resolution potential of surface wave phase velocity measurements at small arrays, *Geophys. J. Int.*, 172, 698-706.

Boschi, L., 2006. Global multiresolution models of surface wave propagation: comparing equivalently regularized Born and ray theoretical solutions, *Geophys. J. Int.*, 167, 238-252.

Brisbourne, A.M. & Stuart, G.W., 1998. Shear-wave velocity structure beneath North Island, New Zealand, from Rayleigh-wave interstation phase velocities, *Geophys. J. Int.*, 133, 175-184.

Dahlen, F. A., S.-H. Hung, and G. Nolet, 2000. Fre´chet kernels for finite-frequency traveltimes, I, Theory, *Geophys. J. Int.*, 141, 157–174.

Deschamps, F., Lebedev, S., Meier, T. & Trampert, J., 2008. Azimuthal anisotropy of Rayleigh-wave phase velocities in the east-central United States, *Geophys. J. Int.*, 173, 827-843.

Ekstrom, G., Tromp, J. & Larson, E.W.F., 1997. Measurements and global models of surface wave propagation, *J. Geophys. Res,* 102, 8137-8157.

Friederich, W., 1998. Wave-theoretical inversion of teleseismic surface waves in a regional network: phase-velocity maps and a three-dimensional upper-mantle shear-wave-velocity model for southern Germany, *Geophys. J. Int.*, 132, 203-225.

Friederich, W., Hunzinger, S. & Wielandt, E., 2000. A note on the interpretation of seismic surface waves over three-dimensional structures, *Geophys. J. Int.*, 143, 335-339.

Laske, G. & Masters, G., 1998. Surface-wave polarization data and global anisotropic structure, *Geophys. J. Int.*, 132, 508-520.

Levshin, A.L., M.P. Barmin, M.H. Ritzwoller, and J. Trampert, 2005. Minor-arc and major-arc global surface wave diffraction tomography, *Phys. Earth Planet. Ints.*, 149, 205-223.

Lin, F.C, Ritzwoller, M.H., Townend, J., Savage, M., & Bannister, S., 2007, Ambient noise Rayleigh wave tomography of New Zealand, *Geophys. J. Int.*, 170, 649-666.

Lin, F.C., Moschetti, M.P. & Ritzwoller, M.H., 2008. Surface wave tomography of the western United States from ambient seismic noise: Rayleigh and Love wave phase velocity maps, *Geophys. J. Int.*, 173, 281-298.

Montelli, R., Nolet, G. & Dahlen, F.A., 2006. Comment on 'Banana-doughnut kernels and mantle tomography' by van der Hilst and de Hoop, *Geophys. J. Int.*, 167, 1204-1210.

Morris, G.B., Raitt, R.W. & Shor, G.G., 1969. Velocity Anisotropy and Delay-Time Maps of Mantle Near Hawaii, *J. Geophys. Res*, 74, 4300.

Moschetti, M.P., M.H. Ritzwoller, and N.M. Shapiro, 2007. Surface wave tomography of the western United States from ambient seismic noise: Rayleigh wave group velocity maps, *Geochem., Geophys., Geosys.*, 8, Q08010, doi:10.1029/2007GC001655.

Nolet, G., 1990. Partitioned wave-form inversion and 2D structure under the NARS array, J. *Geophys. Res*., 95, 8513-8526.

Pollitz, F.F., 2008. Observations and interpretation of fundamental-mode Rayleigh wavefields recorded by the Transportable Array (USArray), submitted to *J. Geophys. Res.*

Prindle, K. & Tanimoto, T., 2006. Teleseismic surface wave study for S-wave velocity structure under an array: Southern California, *Geophys. J. Int.*, 166, 601-621.

Ritzwoller, M.H. and A.L. Levshin, 1998. Eurasian surface wave tomography: Group velocities, *J. Geophys. Res.*, 103, 4839 – 4878.

Ritzwoller, M.H., Shapiro, N.M., Barmin, M.P., & Levshin, A.L., 2002. Global surface wave diffraction tomography, *J. Geophys. Res.*, 107, 2335.

Roth, M., G. Muller, and R. Snieder, 1993, Velocity shift in random media, *Geophys. J. Int.*, 115, 552-563.

Sabra, K.G., P. Gerstoft, P. Roux, and W.A. Kuperman, 2005. Surface wave tomography from microseisms in Southern California, *Geophys. Res. Letts.*, 32, L14311, doi:10.1029/2005GL023155.

Shapiro, N.M. M. Campillo, L. Stehly, and M.H. Ritzwoller, 2005. High resolution surface wave tomography from ambient seismic noise, *Science*, 307(5715), 1615-1618.

Shearer, P. 1999. Introduction to Seismology, Cambridge University Press.

Smith, M.L. & Dahlen, F.A., 1973. Azimuthal Dependence of Love and Rayleigh-Wave Propagation in a Slightly Anisotropic Medium, *J. Geophys. Res.*, 78, 3321-3333.

Smith, W.H.F. & Wessel, P., 1990. Gridding with Continuous Curvature Splines in Tension, *Geophysics*, 55, 293-305.

Smith, D.B., M.H. Ritzwoller, and N.M. Shapiro, 2004. Stratification of anisotropy in the Pacific upper mantle, *J. Geophys. Res.*, 109, B11309, doi:10.1029/2004JB003200.

Trampert J. and Spetzler J., 2006. Surface wave tomography: Finite frequency effects lost in the null space, *Geophys. J. Int.*, 164, 394-400.

Trampert, J., and J.H. Woodhouse, 1996. High resolution global phase velocity distributions, Geophys. Res. Lett., 23, 21-24.

Tromp, J., Tape, C. & Liu, Q.Y., 2005. Seismic tomography, adjoint methods, time reversal and banana-doughnut kernels, *Geophys. J. Int.*, 160, 195-216.

van der Hilst, R.D. & de Hoop, M.V., 2005. Banana-doughnut kernels and mantle tomography, *Geophys. J. Int.*, 163, 956-961.

Van der Lee, S., and A. Frederiksen, 2005. Surface Wave tomography applied to the North American upper mantle, in AGU Monograph "Seismic Earth: Array Analysis of Broadband Seismograms", Eds: Levander A., and G. Nolet, 67-80.

Wielandt, E., 1993. Propagation and Structural Interpretation of Nonplane Waves, *Geophys. J. Int.*, 113, 45-53.

Woodhouse, J.H. & Dziewonski, A.M., 1984. Mapping the Upper Mantle - 3-Dimensional Modeling of Earth Structure by Inversion of Seismic Waveforms, *J. Geophys. Res.*, 89, 5953.

Yang, Y. & Forsyth, D.W., 2006. Rayleigh wave phase velocities, small-scale convection, and azimuthal anisotropy beneath southern California, *J. Geophys. Res.*, 111, B07306.

Yang, Y., M.H. Ritzwoller, A.L. Levshin, and N.M. Shapiro, 2007. Ambient noise Rayleigh wave tomography across Europe, *Geophys. J. Int.*, 168(1), page 259.

Yang, Y., M.H. Ritzwoller, F.-C. Lin, M.P. Moschetti, and N.M. Shapiro, The structure of the crust and uppermost mantle beneath the western US revealed by ambient noise and earthquake tomography, submitted to *J. Geophys. Res.*

Yao, H.J., van der Hilst, R.D. & de Hoop, M.V., 2006. Surface-wave array tomography in SE Tibet from ambient seismic noise and two-station analysis - I. Phase velocity maps, *Geophys. J. Int.*, 166, 732-744.

Yoshizawa, K., and B. L. N. Kennett, 2002. Determination of the influence zone for surface wave paths, *Geophys. J. Int*, 149, 441– 454.

Zhou, Y., Dahlen, F.A. & Nolet, G., 2004. Three-dimensional sensitivity kernels for surface wave observables, *Geophys. J. Int.*, 158, 142-168.

Zhou, Y., Nolet, G., Dahlen, F. A, & Laske, G., 2005. Finite-frequency effects in global surface-wave tomography, *Geophys. J. Int.*, 163, 1087-1111.

Figure Captions

Figure 1.

The 499 stations used in this study are identified by black triangles. Waveforms are taken continuously from October, 2004 until November, 2007. Most stations are from the EarthScope/USArray Transportable Array (TA), but a few exceptions exist, such as NARS Array stations in Mexico. The four red symbols identify locations used later in the paper.

Figure 2.

(a) Great circle paths linking all station R06C (southeast of Lake Tahoe, identified by the white star) with all TA stations where cross-correlations were obtained. (b) Symmetric component record section for 15-30 sec period band-passed vertical-vertical cross-correlations with station R06C in common. More than 450 cross-correlations are shown. Clear move-out near 3km/s is observed.

Figure 3.

Snapshots of the amplitude of the ambient noise cross-correlation wavefield with TA station R06C in common at the center. Each of the 15-30 sec band-passed cross-correlations is first fit with an envelope function in the time domain and the envelope function amplitudes are then interpolated spatially. Two instants in time are shown, illustrating clear move-out and the unequal azimuthal distribution of amplitude.

Figure 4.

(a) The phase travel time surface for the 24 sec Rayleigh wave centered on TA station R06C. Contours are separated by 24 sec intervals. (b) The difference in phase speed travel time using two different phase-front interpolation schemes. The 48 sec contour is identified with a grey circle centered on station R06C.

Figure 5.

Rayleigh wave phase speed travel time surfaces at periods of (a,b) 24 sec and (c,d) 12 sec centered on stations R06C (eastern California) and F10A (northeastern Oregon). Travel time level lines are presented in increments of the wave period. The maps are truncated within 2 wavelengths of the central station and where the three out of four quadrant selection criterion is not satisfied,.These two criteria usually take effect near the periphery of the station coverage.

Figure 6.

(a) The phase speed inferred from the Eikonal equation for the 24 sec Rayleigh wave travel time surface shown in Fig. 5a centered on station R06A. (b) The propagation direction determined from the gradient of the phase travel time surface at each point is shown with arrows. The difference between the observed propagation direction and the straight ray prediction (radially away from stations R06A0 is shown as the background color.

Figure 7.

(a) Example of the azimuthal distribution of the Rayleigh wave phase velocity measurements at 24 sec period for the point in central Nevada indicated by the star in Figure 1. (b) Same as (a), but for the 12 sec Rayleigh wave phase speed at the same location. The mean and standard deviation of the mean are identified at upper left in each panel.

Figure 8.

(a) The 24 sec period isotropic Rayleigh wave phase speed uncertainty map, determined from the distribution of phase speed measurements based on applying the Eikonal equation to each of the phase travel time maps at each point. (b) The 12 sec isotropic Rayleigh wave phase speed uncertainty map.

Figure 9.

(a) The 24 sec Rayleigh wave isotropic phase speed map derived from Eikonal

tomography. The isotropic phase speed at each point is calculated from the distribution of local phase speeds determined from each of the phase travel time maps. (b) Same as (a), but the straight ray inversion of Barmin et al. (2001) is used. The black line is the 100 km resolution contour. (c) The difference between Eikonal and straight ray tomography is shown where positive values indicate that the Eikonal tomography gives a higher local phase speed.

Figure 10.

The same as Figure 9, but for the 12 sec Rayleigh wave. The result of Eikonal tomography is slightly slower (yellow-red shades), on average, than the straight ray tomography because it models off-great-circle propagation.

Figure 11.

Normalized histograms of the Rayleigh wave phase speed difference across the studied region between Eikonal tomography and straight ray tomography at 12 and 24 sec period. The mean differences result because Eikonal tomography models off-great-circle propagation, which is more significant at 12 than 24 sec period.

Figure 12.

(a) An example of the spatial coherence of the measurements for the 24 sec Rayleigh wave at the point in central Nevada indicated by the star in Figure 1. (b) The best fitting cone to the surface in (a). (c) The radius (R) of the best fitting cone at each location, which bears a similarity to resolution.

Figure 13.

Examples of the azimuthal dependence of phase velocity measurements for the 24 sec Rayleigh wave at four points in the western US where large amplitude 2ψ azimuthal variation can be observed: (a) Utah, (b) Nevada, (c) northern California, and (d) central California. The locations are indicated by the circle, star, square, and diamond in Figure 1, respectively. Error bars are estimated based on the distribution of phase velocity measurements in each 20^{o} azimuthal bin for the given location and its 8 nearest

neighboring grid points. For each case, the solid line is the best fit of the 2ψ azimuthal variation.

Figure 14.

(a) The 24 sec period Rayleigh wave azimuthal anisotropy fast axis directions and peak-to-peak amplitudes, $2A/c_0$, which are proportional to the length of the bars. (b) Peak-to-peak amplitude of anisotropy presented in percent.

Figure 15.

(a) Variance reduction of the 2ψ azimuthal anisotropy relative to the isotropic speed at each point. (b) The uncertainty in the angle of the fast direction, φ. (c) The uncertainty of the amplitude of anisotropy.

Figure 16.

(a)-(b) Same as Figure 14(a)-(b), but here the 24 sec Rayleigh wave azimuthal anisotropy result is determined with the traditional straight ray method of Barmin et al. (2001) with a regularlization chosen approximate the amplitudes in Fig. 14b. (c) The normalized histogram of the difference in fast directions between the Eikonal tomography result (Fig. 14a) and the straight ray tomography result. (d)-(f) same as (a)-(c) but with stronger smoothing regularization. Patterns of anisotropy remain largely unchanged, but amplitudes diminish with greater the damping.

Figure 17.

Same as Figure 14, but for the 12 sec Rayleigh wave.

Figure 18.

Same as Figure 16, but for the 12 sec Rayleigh wave. Agreement between the Eikonal and straight ray tomography is worse at 12 sec than 24 sec because of the larger effect of off-great-circle propagation.

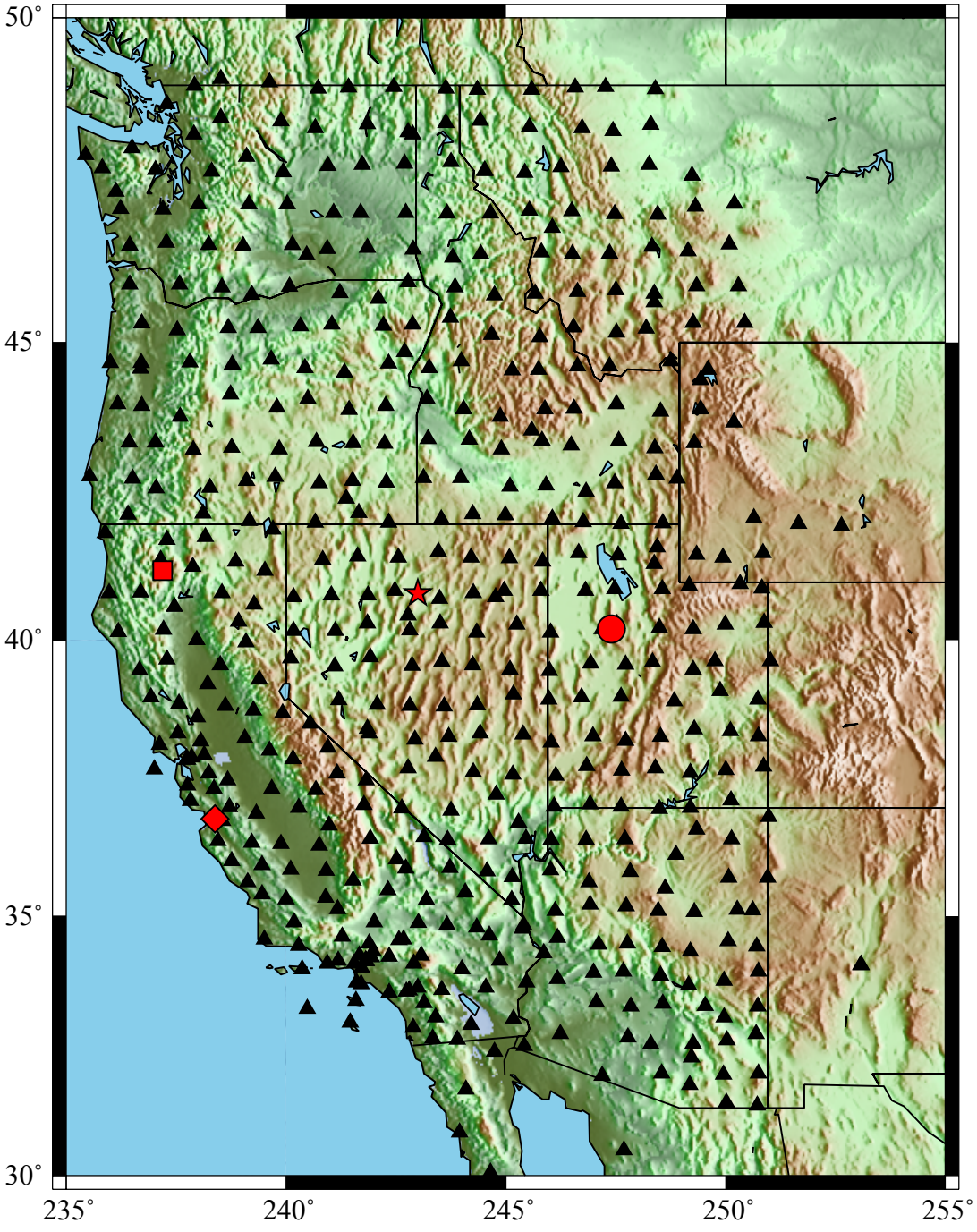

Figure 1

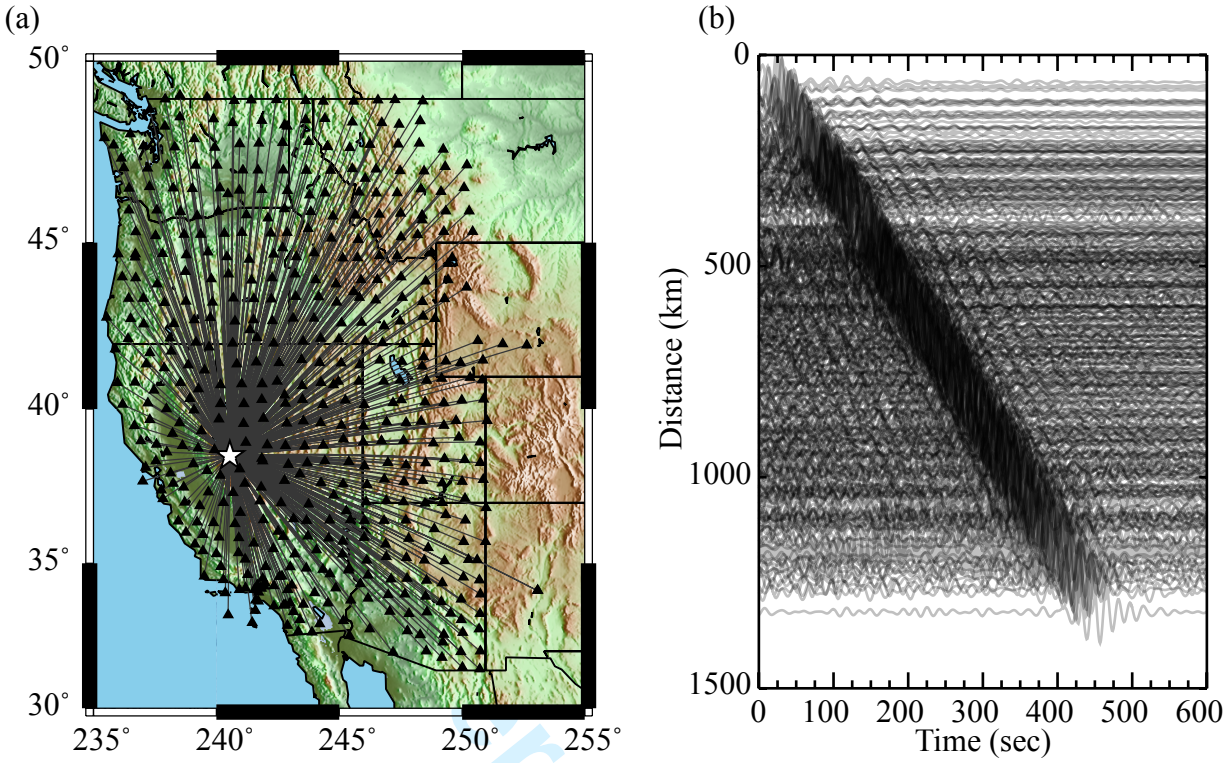

Figure 2

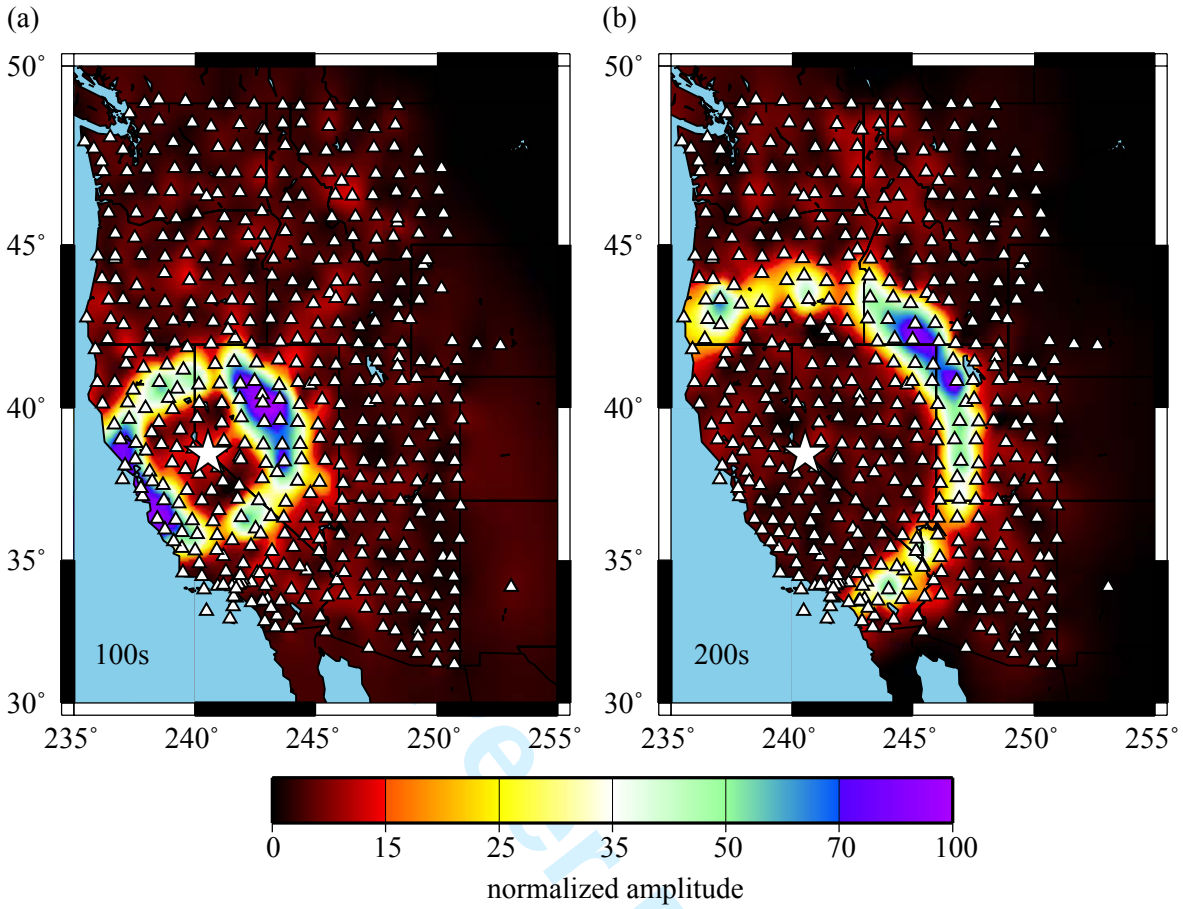

Figure 3

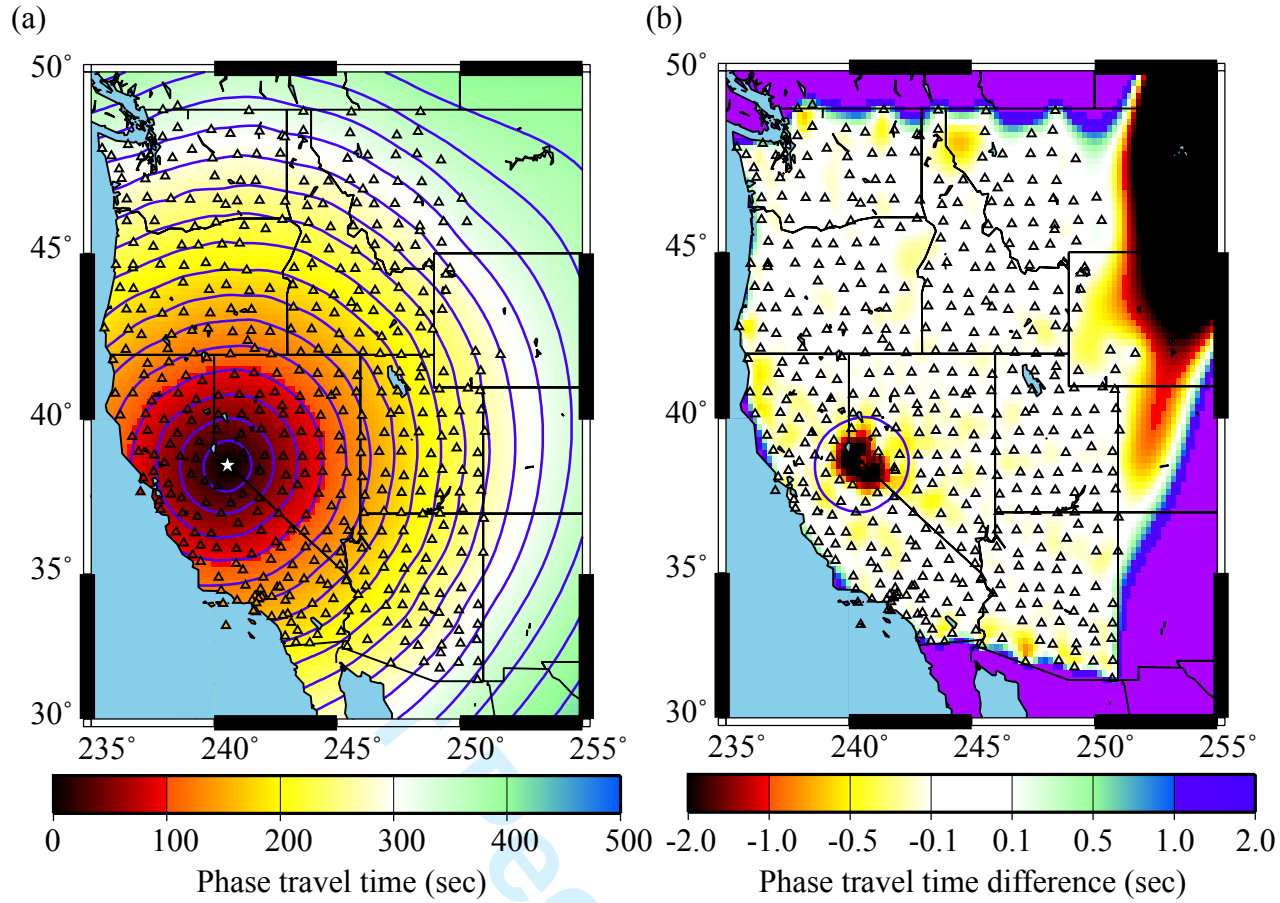

Figure 4

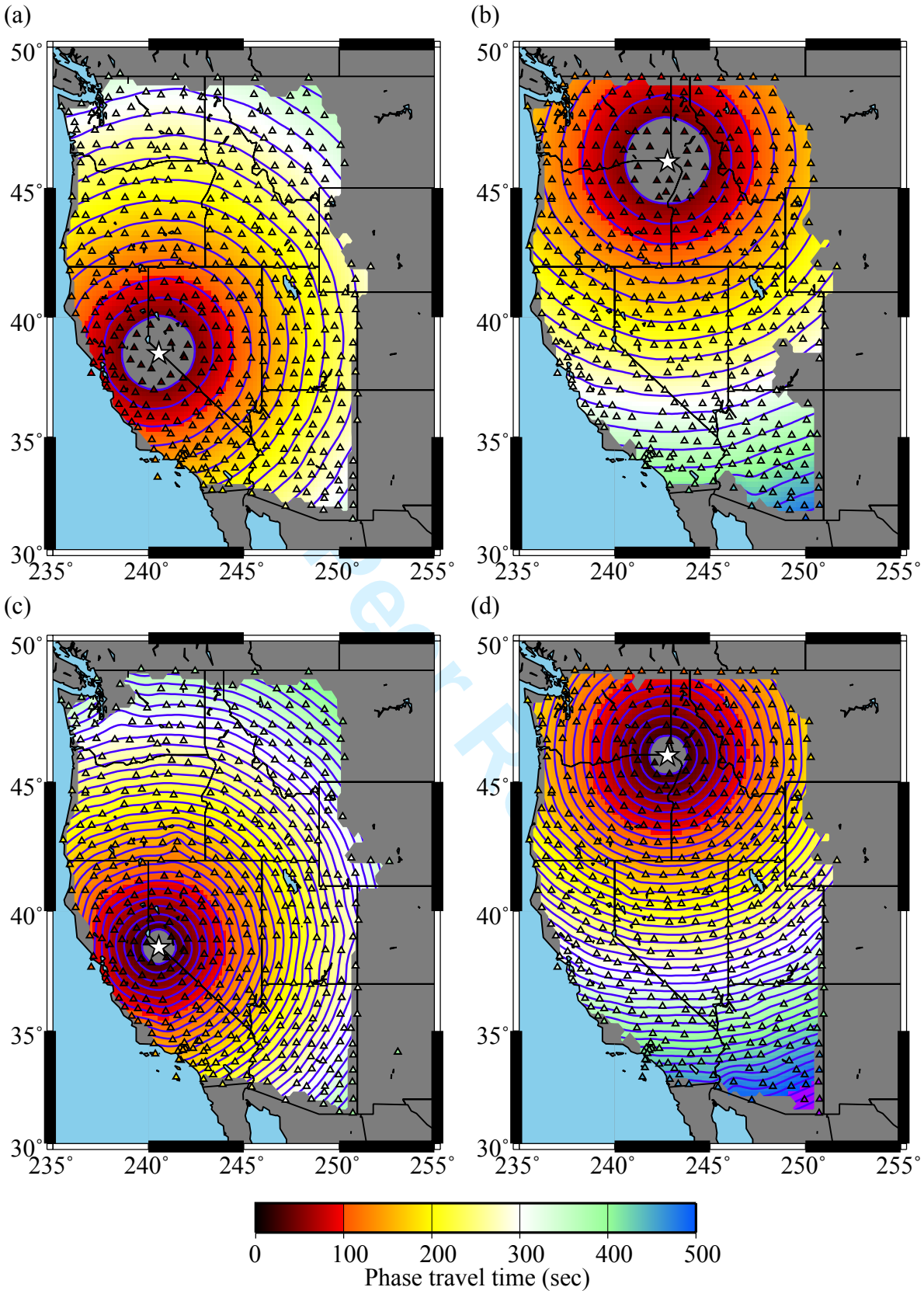
(a)
(b)
(c)
(d)
50°
45°
40°
35°
30°
235°
240°
245°
250°
255°
0
100
200
300
400
500
Phase travel time (sec)

Figure 5

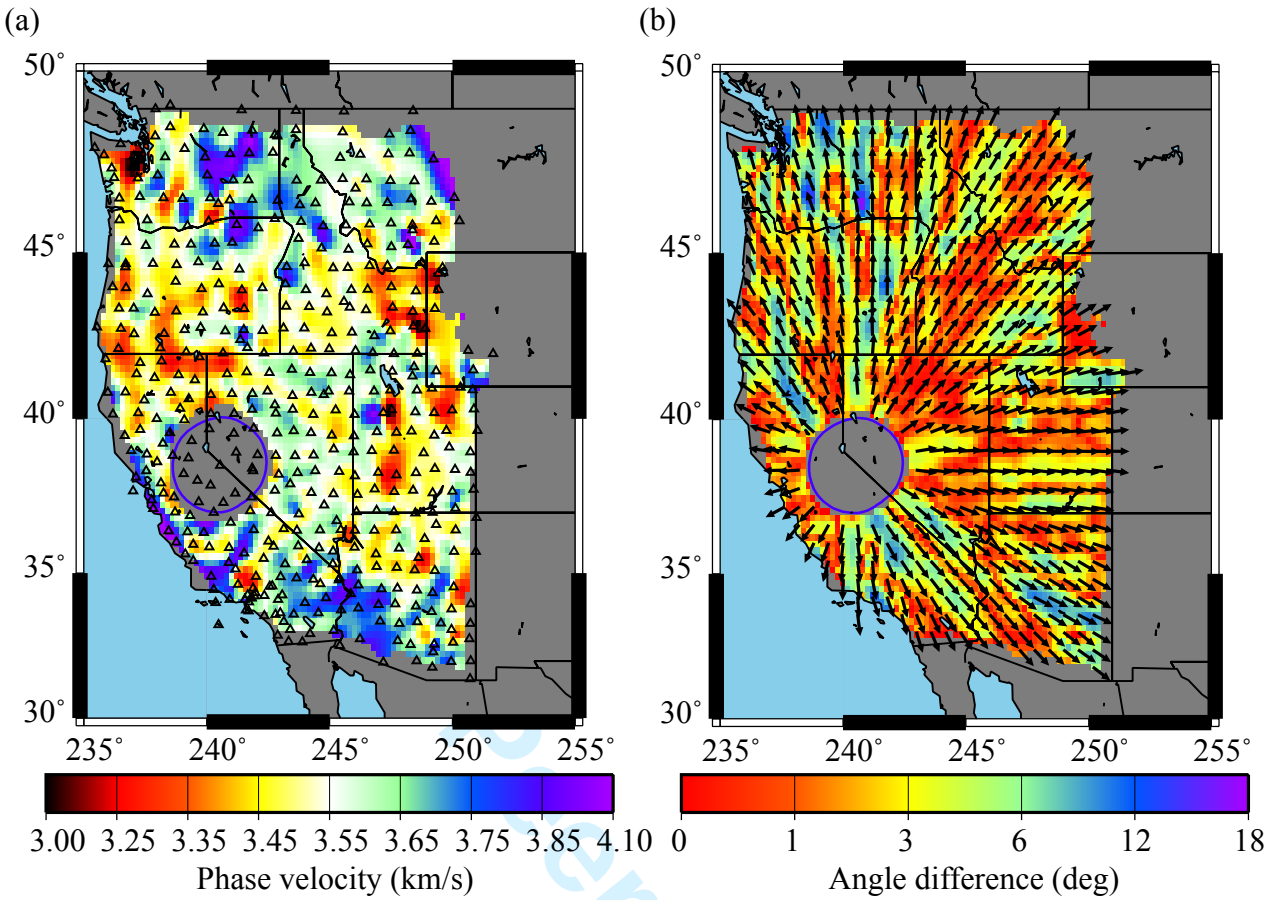

Figure 6

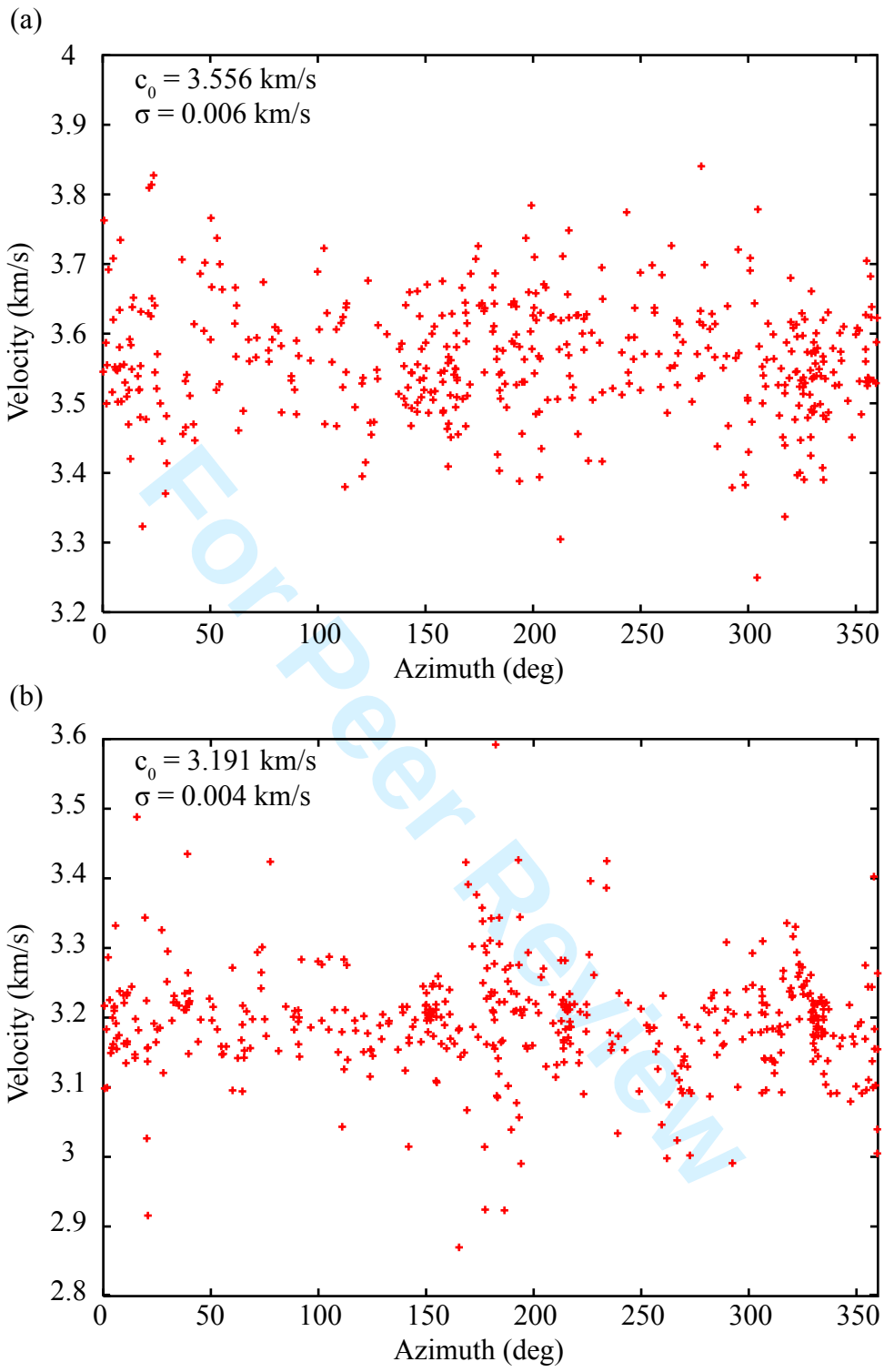

Figure 7

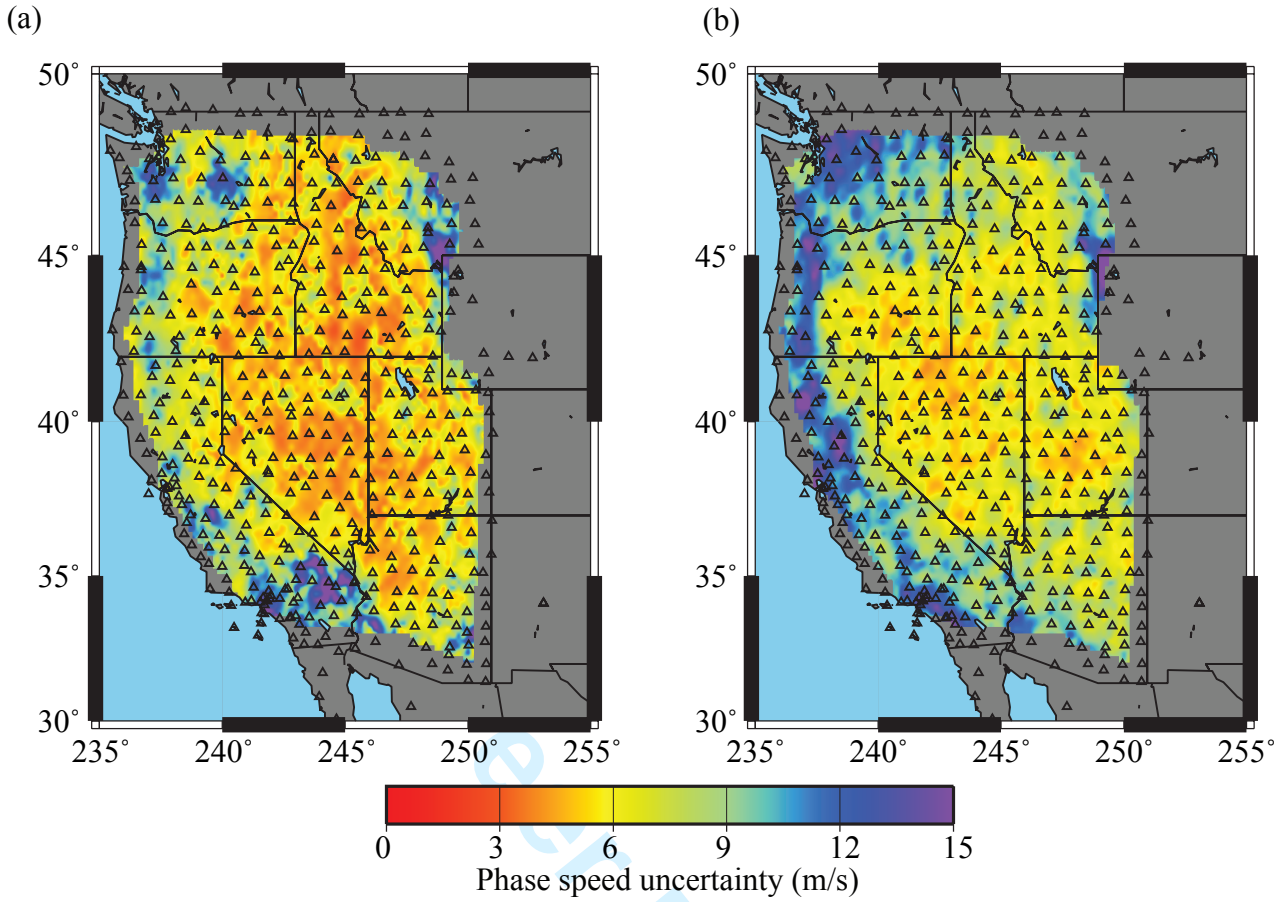

Figure 8

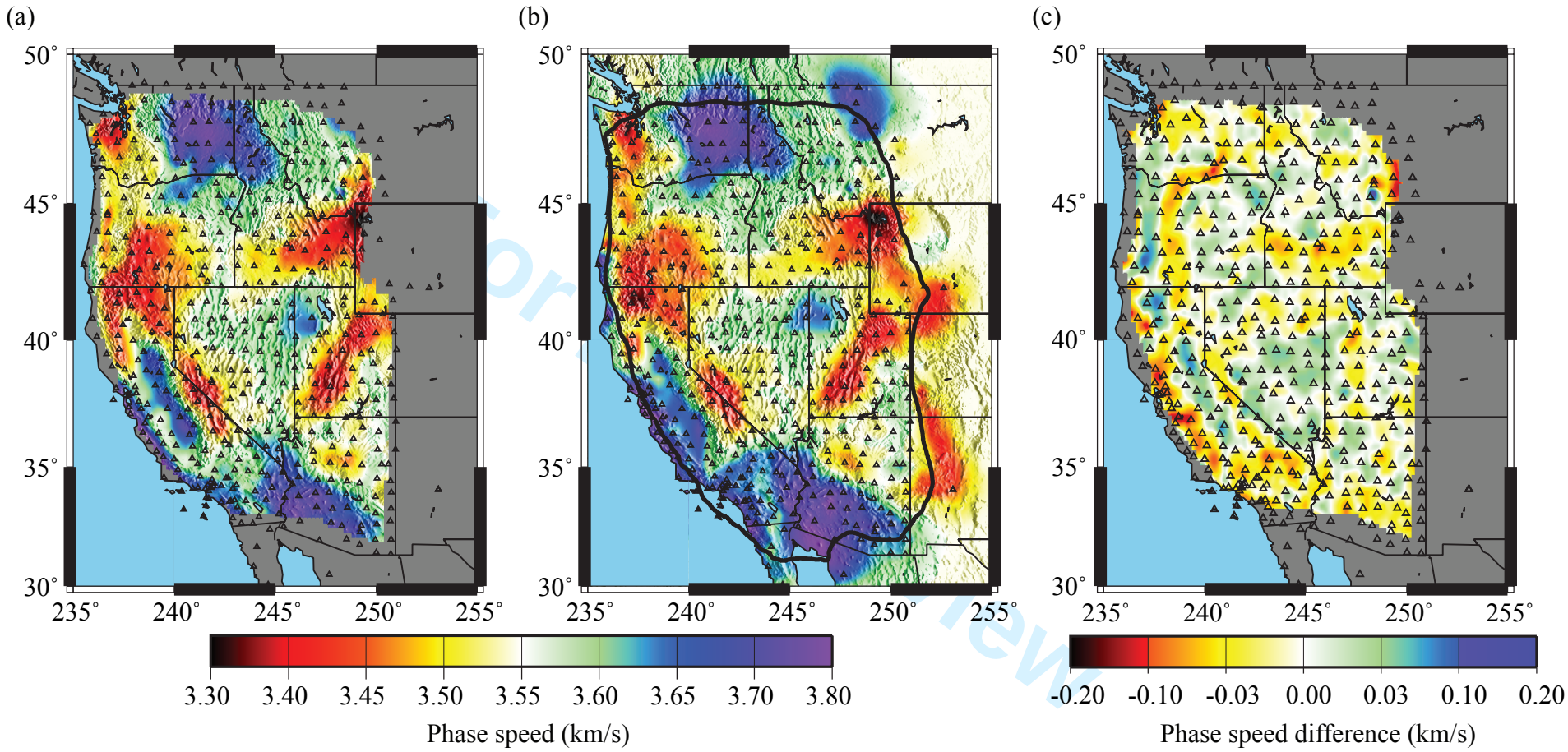
(a)
(b)
(c)
50°
45°
40°
35°
30°
235°
240°
245°
250°
255°
3.30
3.40
3.45
3.50
3.55
3.60
3.65
3.70
3.80
Phase speed (km/s)
-0.20
-0.10
-0.03
0.00
0.03
0.10
0.20
Phase speed difference (km/s)

Figure 9

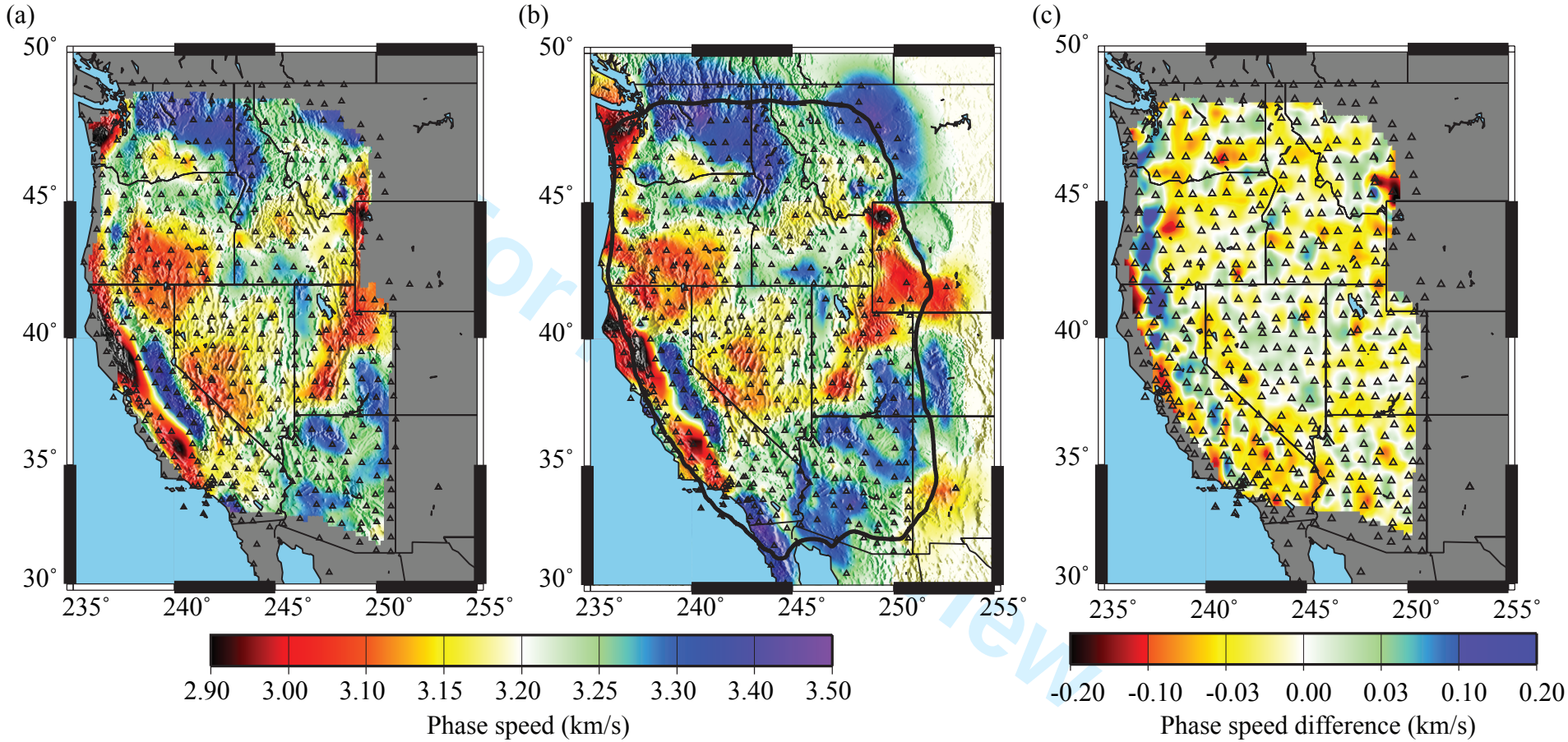
(a)
(b)
(c)
50°
45°
40°
35°
30°
235°
240°
245°
250°
255°
2.90
3.00
3.10
3.15
3.20
3.25
3.30
3.40
3.50
Phase speed (km/s)
-0.20
-0.10
-0.03
0.00
0.03
0.10
0.20
Phase speed difference (km/s)

Figure 10

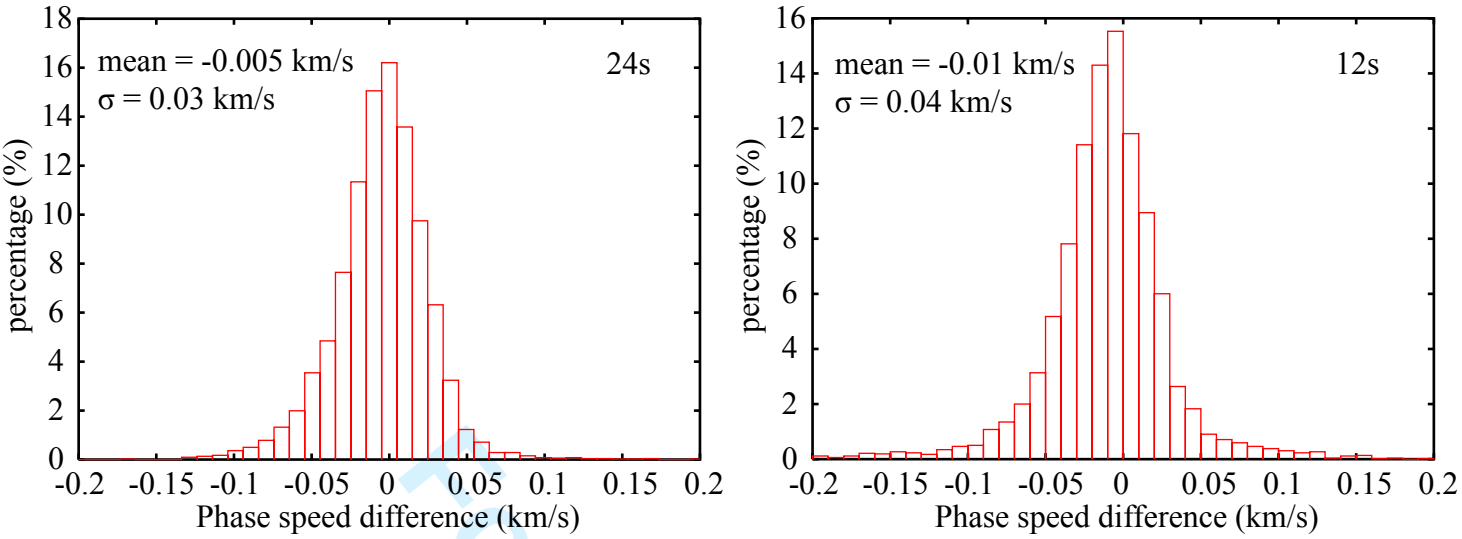

Figure 11

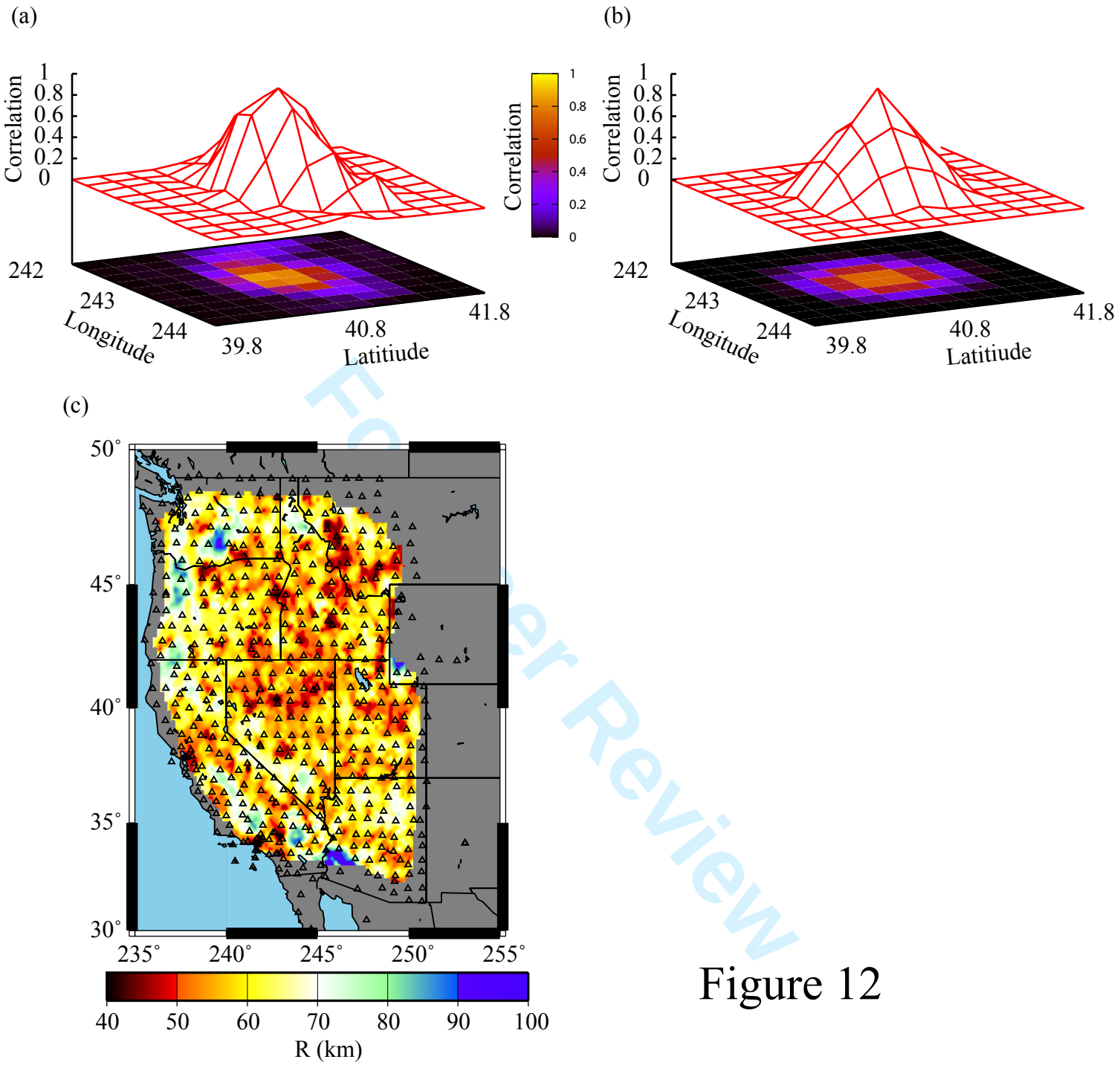

Figure 12

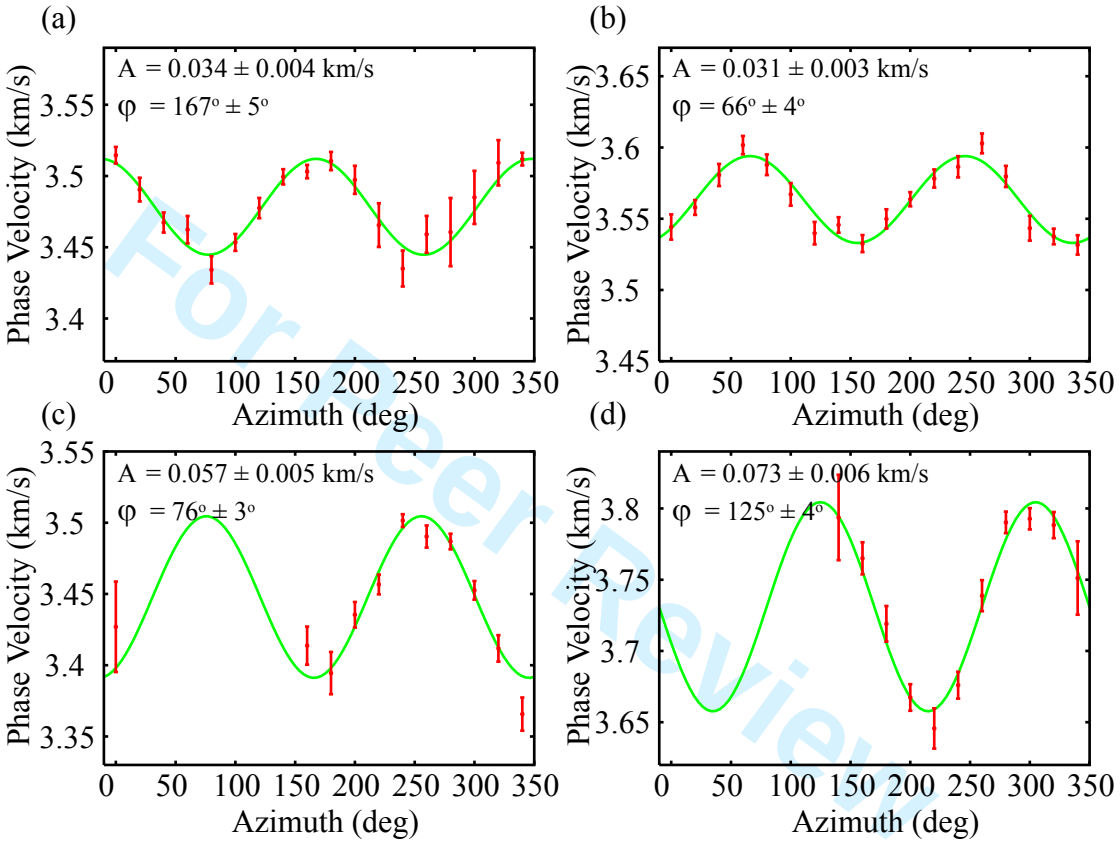

Figure 13

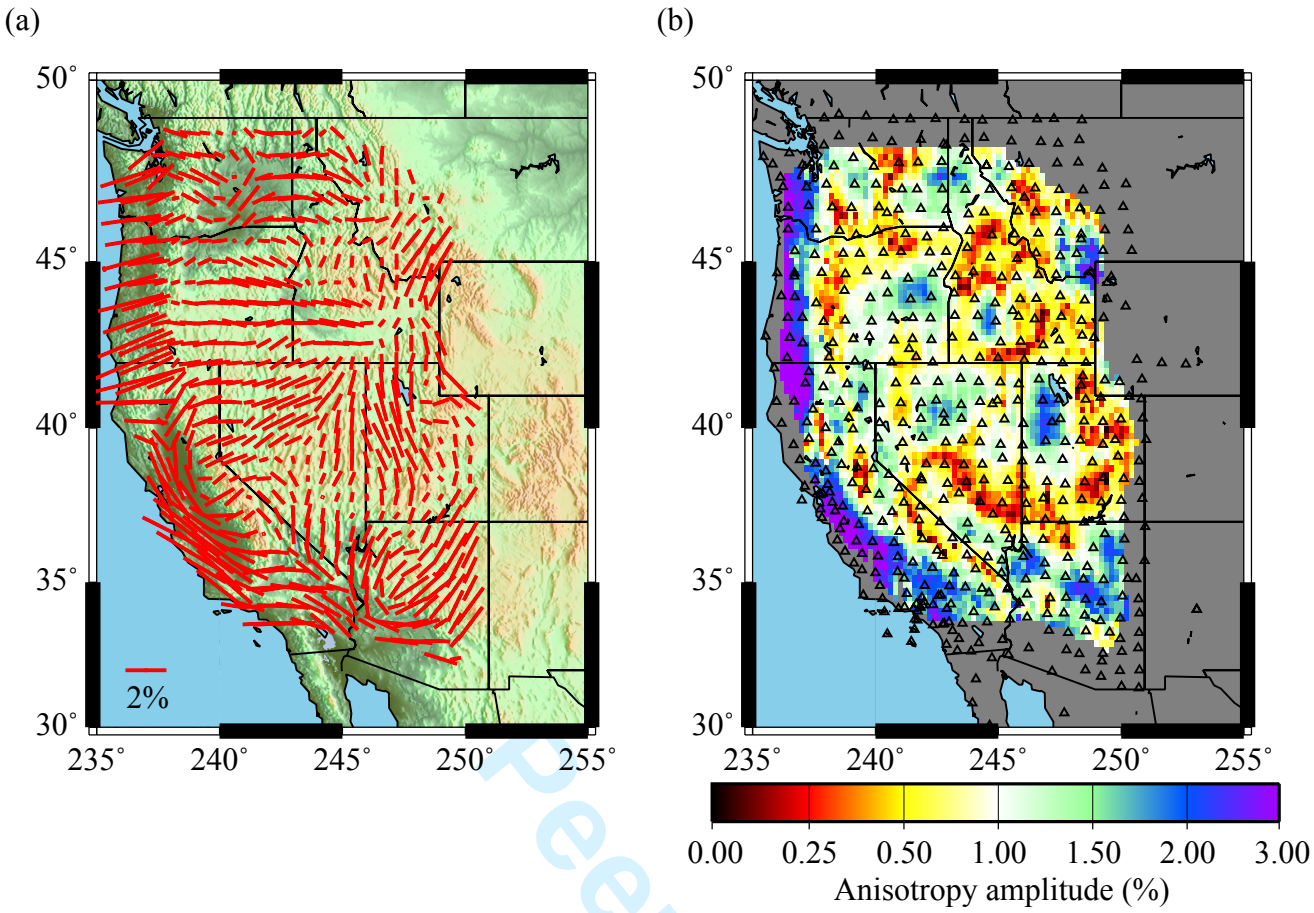

Figure 14

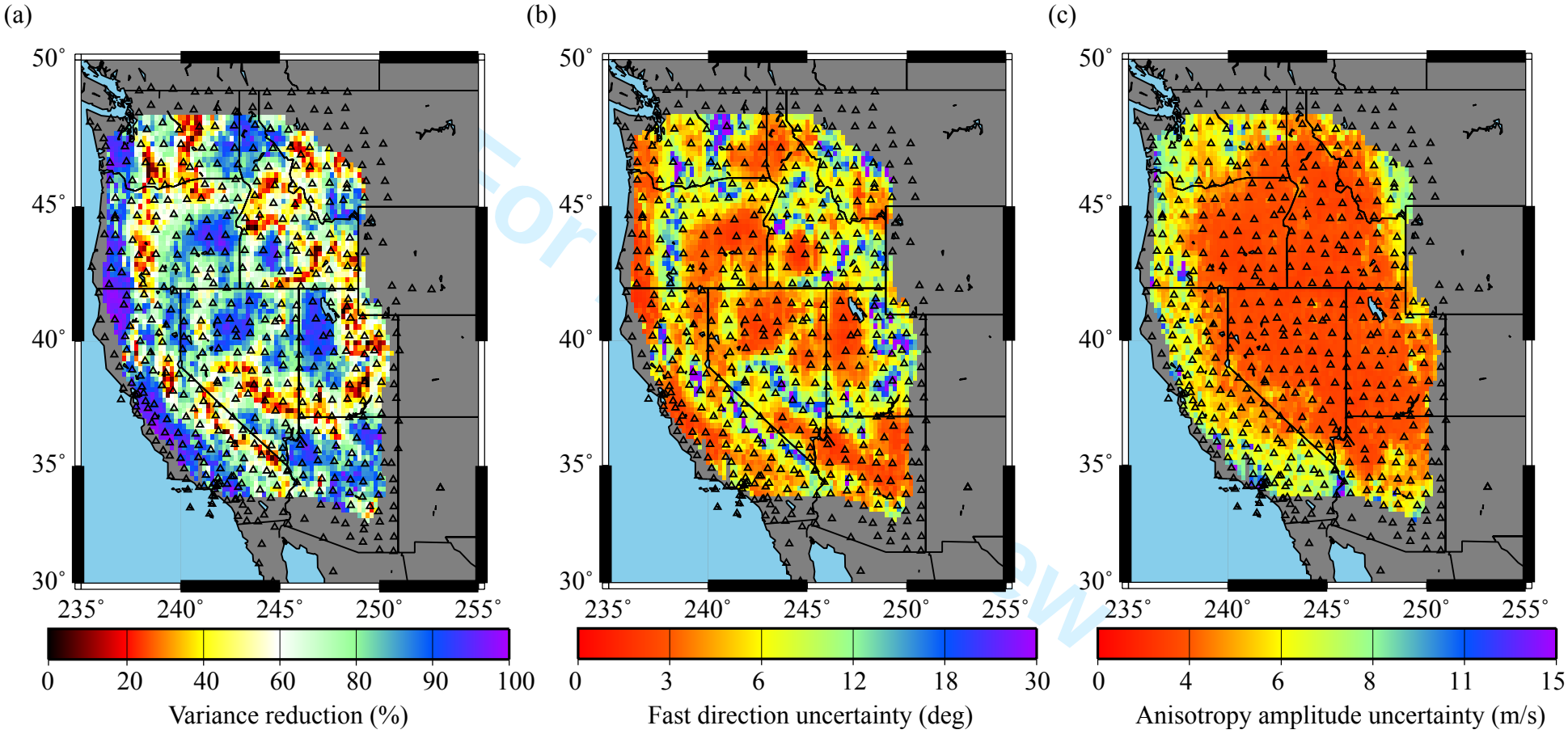
(a)
(b)
(c)
50°
45°
40°
35°
30°
235°
240°
245°
250°
255°
0
20
40
60
80
90
100
Variance reduction (%)
0
3
6
12
18
30
Fast direction uncertainty (deg)
0
4
6
8
11
15
Anisotropy amplitude uncertainty (m/s)

Figure 15

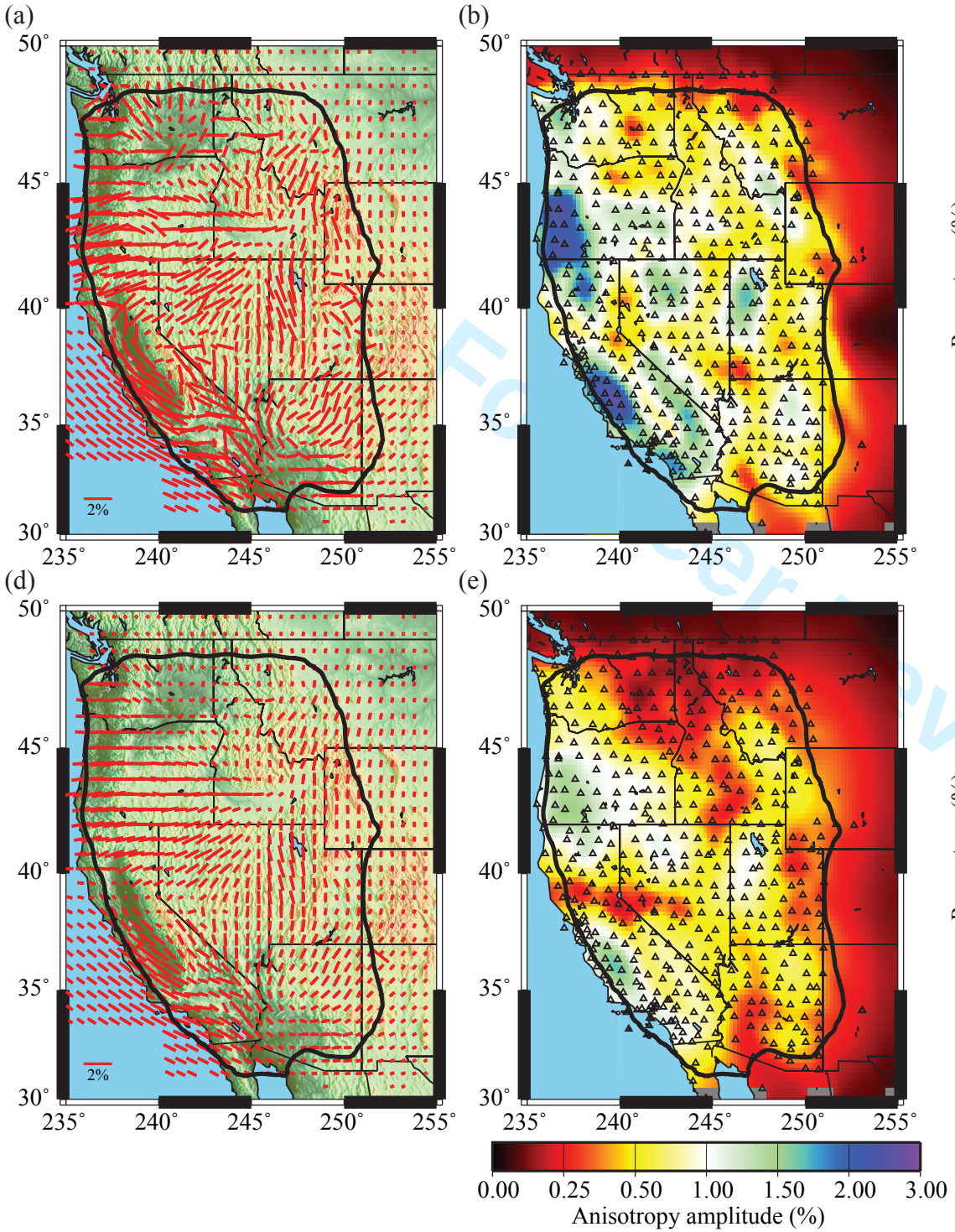

Fiugre 16

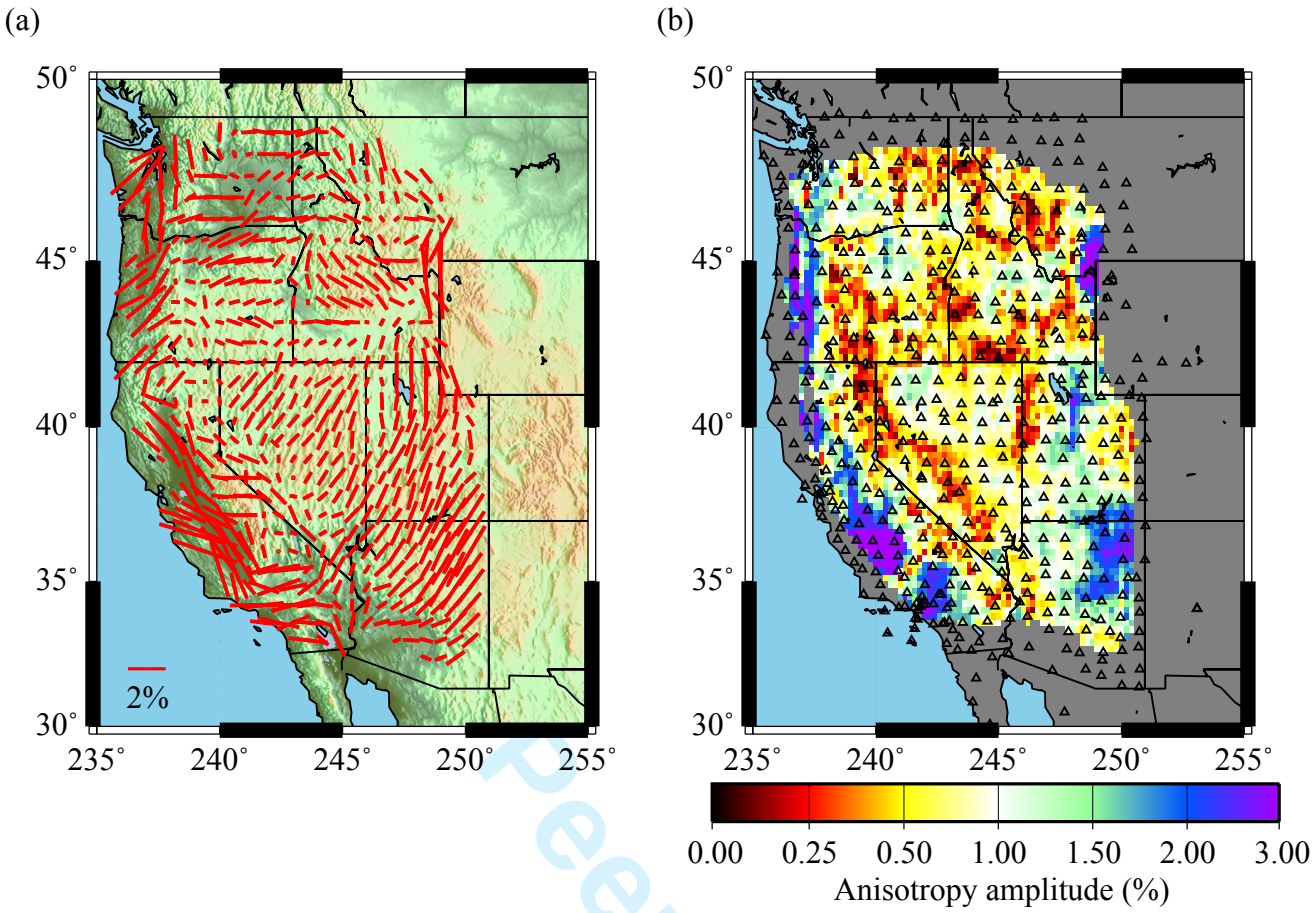

Figure 17

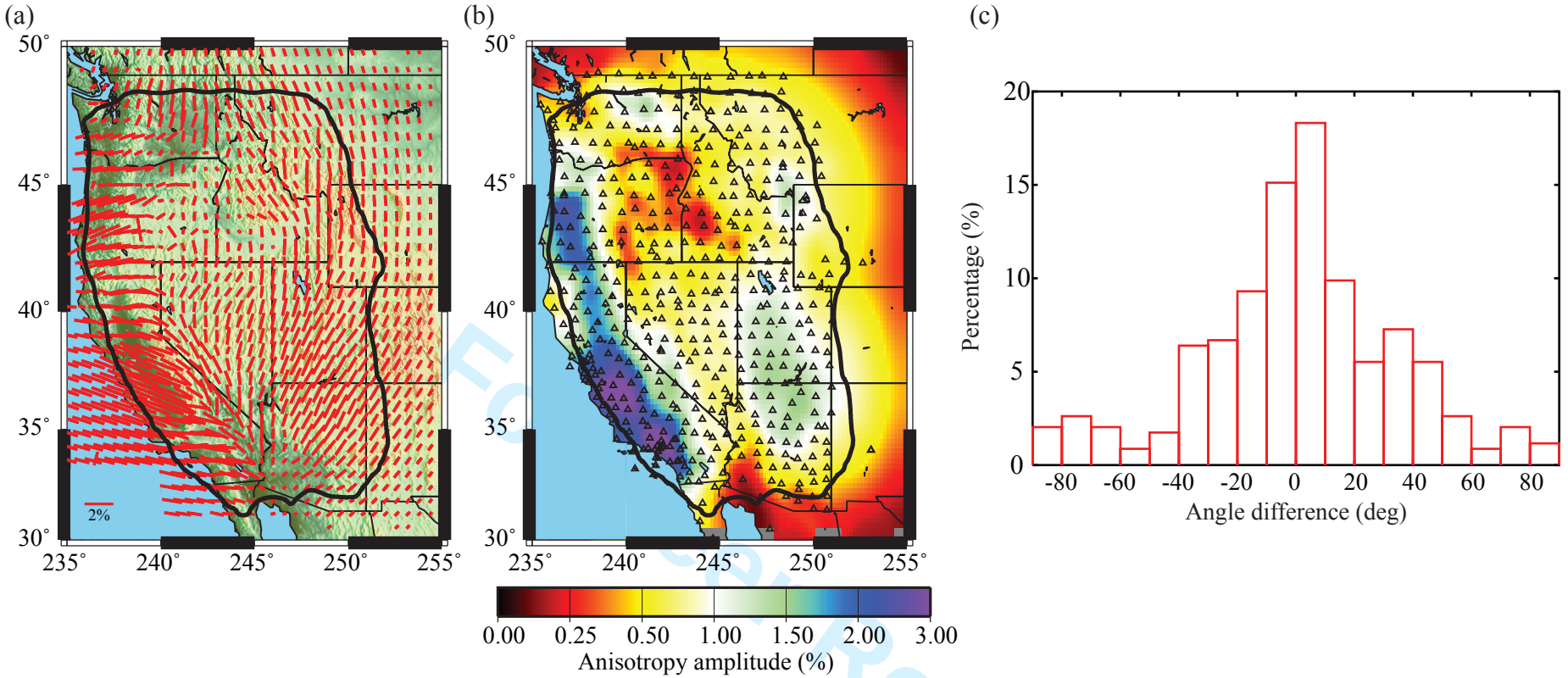

Fiugre 18